Nonlinear Dyn (2019) 98:703–734
https://doi.org/10.1007/s11071-019-05223-y

ORIGINAL PAPER

A dual family of dissipative structure-dependent integration methods for structural nonlinear dynamics

Shuenn-Yih Chang

Received: 9 January 2018 / Accepted: 28 August 2019 / Published online: 14 September 2019

Abstract A dual family of dissipative structure-dependent integration methods is proposed for structural nonlinear dynamics. It not only can be a family of two-step integration methods but also can be a family of one-step integration methods correspondingly. This family of methods is derived from an ingenious arrangement of the displacement difference equation, where the previous step data are applied to replace the previous two-step data by means of the asymptotic equation of motion. It has desirable properties, such as unconditional stability, explicitness of each time step, second-order accuracy and high-frequency numerical damping. In addition, it has no adverse properties that have been found in some structure-dependent integration methods, such as weak instability, conditional stability for stiffness hardening systems, high-frequency overshooting in steady-state responses and poor capability of seizing high nonlinearity. This family of methods contains most current semi-explicit, structure-dependent integration methods as it is a family of two-step integration methods although it also covers many brand-new members of two-step integration methods, and it is a brand-new family of one-step integration methods. It has the same properties as those of the generalized-α method for linear elastic systems. However, it saves many computational efforts for solving inertial problems due to no involvement of nonlinear iterations per time step.

Keywords Unconditional stability · Numerical dissipation · Explicit formulation · Accuracy · Nonlinear dynamic analysis · Structure-dependent integration method

S. Chang (✉)
Department of Civil Engineering, National Taipei University of Technology, NTUT Box 2653, No. 1, Section 3, Jungshiau East Road, Taipei 10608, Taiwan, Republic of China
e-mail: changsy@ntut.edu.tw

1 Introduction

Time integration methods are often applied to solve the discretized equations of motion. Many integration methods have been successfully developed for structural dynamics applications, such as the Houbolt method [1], Newmark method [2], Wilson-θ method [3], Park method [4], HHT-α method [5], WBZ-α method [6], generalized-α method [7], Chang α-function method [8], the methods developed by Tamma et al. [9–12] and many other methods [13–21]. An integration method must be a convergent method [22–24] and the convergence is referred to stability and consistency based on the Lax equivalence theory [25]. In general, numerical damping can be used to extinguish the spurious oscillations of the unresolved high-frequency modes caused by spatial discretization. In addition, the convergence of nonlinear iterations can be improved if numerical damping is used to remove the spurious growth of the high-frequency modes in solving highly nonlinear problems. As a result, it is

advantageous for an integration method to have controllable numerical dissipation to solve inertial problems, where the total response is governed by low-frequency modes, while the high-frequency responses are of no interest. Some integration methods have been developed to have desired numerical damping, such as the Wilson-θ method [3], HHT-α method [5], WBZ-α method [6], the generalized-α method [7], Chang α-function method [8], and the methods developed by Tamma et al. [9–12].

The numerical properties, such as explicitness, unconditional stability, second-order accuracy, high-frequency numerical damping, and no overshoot, are often desired for an integration method. However, it was shown by Dahlquist [26] that there is no explicit, unconditionally stable method among the linear multi-step methods. Hence, there is no conventional integration methods, whose coefficients of the difference equations are scalar constants, that can combine explicit formulation and unconditional stability together. This Dahlquist barrier is inapplicable to structure-dependent integration methods because their coefficients of the difference equations methods are no longer limited to be scalar constants but can be matrices of the initial structural properties and time step. In fact, some structure-dependent integration methods have been proposed for time integration. They not only have unconditional stability but also explicit formulation [27–34] although they possess no numerical damping. Some families of the structure-dependent integration methods were developed to have desirable numerical damping in addition to unconditional stability and explicit formulation [35–37]. The main drawback of the Chang family methods [35,36] is that they are two-step methods, and a distinct starting procedure is needed for time integration. Although the KR-α method [37] is a one-step method, it possesses some adverse properties [38], such as a weak instability, a conditional stability for stiffness hardening systems, and a high-frequency overshoot in steady-state responses.

Two adverse properties are generally found for structure-dependent integration methods. One is that unconditional stability can be achieved only for linear elastic and stiffness softening systems but not for stiffness hardening systems [39] and the other is that an adverse overshoot may occur in high-frequency steady-state responses [40]. A stability amplification factor has been employed to improve the conditional stability property for stiffness hardening systems [39]. Besides, a loading term has been introduced into the displacement and/or velocity difference equations to get rid of the adverse high-frequency overshoot in steady-state responses [40]. In this work, both techniques are used to develop a dual family of structure-dependent integration methods, which can be a family of one-step or two-step integration methods. This family of methods covers most structure-dependent integration methods proposed by Chang [27–30,35,36]. It can inherit the favorable properties from general structure-dependent integration methods, such as a second-order accuracy, the explicitness of each time step, an unconditional stability for linear elastic and stiffness softening systems and an efficient computing, while it has no adverse properties, such as a conditional stability for stiffness hardening systems, a high-frequency overshoot in steady-state responses and no weak instability. The basic assumptions and details for developing a new family of structure-dependent integration methods are presented. Numerical properties of this family of methods are explored for both linear and nonlinear systems. In addition, nonlinear examples are also applied to confirm the feasibility, numerical properties and computational efficiency. Finally, one non-dissipative subfamily and two dissipative subfamilies of this family of methods are also presented and discussed.

2 Development

In structural dynamics or earthquake engineering, the differential equation of motion for a single degree of freedom can be expressed as:

$$m\ddot{u} + c\dot{u} + ku = f \tag{1}$$

where f, k, c, and m are the external force, stiffness, viscous damping coefficient, and mass, respectively; and $\ddot{u}$, $\dot{u}$ and u are the acceleration, velocity, and displacement, respectively. In general, an initial-value problem is to find a solution of this equation to satisfy the specified initial conditions. An integration method can be applied to solve Eq. (1), and it generally consists of the equation of motion and two difference equations, where one is for displacement and the other is for velocity. This structure is adopted in this work for developing a new family of methods.

2.1 Prerequisite techniques

Two techniques will be applied to develop the new family of methods. One is a loading term [40] and the other is a stability amplification factor [39]. Structure-dependent integration methods in early development involve no loading term in either displacement or velocity difference equation, and thus an overshoot in steady-state responses is found, and it becomes significant as the product of the natural frequency and step size increases. A remedy has been proposed by introducing a loading term into the displacement and/or velocity difference equation to eliminate the adverse overshoot in steady-state responses. In general, this loading term can be determined from the local truncation error of an integration method.

Most structure-dependent integration methods [27–33,35,36] can have unconditional stability for linear elastic and stiffness softening systems, while they become conditionally stable for stiffness hardening systems. A parameter has been introduced to monitor the stiffness change and called the instantaneous degree of nonlinearity [28–30]. It is defined as ratio $\delta_{i+1} = k_{i+1}/k_0$, where k_{i+1} is the stiffness at the end of the $(i+1)$th time step. A case of $\delta_{i+1} = 1$ indicates the instantaneous stiffness at the end of the $(i+1)$th time step equal to the initial stiffness. A stiffness hardening of $\delta_{i+1} > 1$ implies that the instantaneous stiffness is larger than the initial stiffness at the end of the $(i+1)$th time step, and a stiffness softening case of $0 < \delta_{i+1} < 1$ implies that the instantaneous stiffness is less than the initial stiffness. In general, a structure-dependent integration method can only have an unconditional stability in the interval of $\delta_{i+1} \leq 1$ while it becomes conditionally stable as $\delta_{i+1} > 1$. This property will cause an inconvenience or limitations since δ_{i+1} might not be known as a priori before dynamic analysis [27–33,35,36]. Hence, a stability amplification factor σ has been used to augment an unconditional stability interval. The concept to propose such a technique originates from the virtual enlargement of k_0 [39]. This is because that an unconditional stability interval can be augmented if the initial stiffness is virtually modified from k_0 to σk_0. Thus, the unconditional stability interval will be amplified from $k_{i+1} \leq k_0$ to $k_{i+1} \leq \sigma k_0$ because a structure- dependent integration method generally has an unconditional stability interval of $\delta_{i+1} \leq 1$.

2.2 Two-step method

Since a structure-dependent integration method can generally combine unconditional stability and explicit formulation together [27–36], it is chosen for this development. An asymptotic equation of motion and the velocity difference equation involved in the Newmark family method have been used to successfully develop many families of dissipative integration methods, such as the HHT-α method, WBZ-α method and generalized-α method. Thus, both are adopted herein for developing a new family of dissipative, structure-dependent integration methods. Meanwhile, two prerequisites must be assumed for the proposed displacement difference equation so that the developed family of structure-dependent integration methods is semi-explicit and dissipative. One is to have an explicit formulation and the other is to have structure-dependent coefficients. In the pilot study, a one-step, structure-dependent displacement difference equation is assumed at first. However, it is unable to yield such a displacement difference equation to form a family of structure-dependent integration methods that has desired numerical properties. As an alternative, a two-step displacement difference equation is assumed. In fact, the proposed family of methods is expressed as:

$$
\begin{aligned}
&(1-\alpha_1)\, m a_{i+1} + \alpha_1 m a_i + (1-\alpha_2)\, c v_{i+1} \\
&\quad + \alpha_2 c v_i + (1-\alpha_3)\, k d_{i+1} + \alpha_3 k d_i \\
&\quad = (1-\alpha_3)\, f_{i+1} + \alpha_3 f_i \\
&d_{i+1} = d_i + \beta_1 (\Delta t)\, v_i + \beta_2 (\Delta t)^2 a_i \\
&\quad + \beta_3 \left[\alpha_1 (\Delta t)^2 a_{i-1} + \alpha_2 2\xi \Omega_{i-1} (\Delta t)\, v_{i-1} \right. \\
&\quad \left. + \alpha_3 \Omega_{i-1}^2 d_{i-1} - \alpha_3 F_{i-1} \right] + p_{i+1} \\
&v_{i+1} = v_i + (\Delta t) \left[(1-\gamma)\, a_i + \gamma a_{i+1} \right]
\end{aligned}
\tag{2}
$$

where $\Omega_{i-1} = \omega_{i-1}(\Delta t)$ and the natural frequency $\omega_{i-1} = \sqrt{k_{i-1}/m}$ is determined from the stiffness k_{i-1} at the end of the of $(i-1)$th time step; and f_i, a_i, v_i, and d_i are the nodal external force, acceleration, velocity and displacement, respectively. In addition, $F_{i-1} = \frac{1}{m}(\Delta t)^2 f_{i-1}$ is defined for brevity and ξ is a viscous damping ratio. Notice that p_{i+1} is a function of dynamic loading and thus it is a loading term, which has never been found in a conventional difference equation and can be used to remove a high-frequency overshoot in steady-state responses [40]. The parameters α_1 to α_3 are scalar constants, while β_1 to β_3 are structure-dependent coefficients. Although α_2 is

assumed to be different from α_3 at first, it was manifested from the local truncation error that the choice of $\alpha_2 = \alpha_3$ can have a better order of accuracy. Thus, $\alpha_2 = \alpha_3$ is adopted subsequently.

It is seen in Eq. (2) that the displacement difference equation is a two-step difference equation since the previous two-step data are involved. Notice that an ingenious arrangement of the step data of the $(i-1)$th time step is intended to transform the two-step displacement difference equation into a one-step displacement difference equation by applying the asymptotic equation of motion. In fact, the asymptotic equation of motion after adopting $\alpha_2 = \alpha_3$ can be alternatively written as:

$$\begin{aligned}&\alpha_1 (\Delta t)^2 a_{i-1} + \alpha_2 2\xi\Omega_{i-1} (\Delta t) v_{i-1} \\ &\quad + \alpha_2 \Omega_{i-1}^2 d_{i-1} - \alpha_2 F_{i-1} = -(1-\alpha_1)(\Delta t)^2 a_i \\ &\quad - (1-\alpha_2) 2\xi\Omega_i (\Delta t) v_i \\ &\quad - (1-\alpha_2)\Omega_i^2 d_i + (1-\alpha_2) F_i \end{aligned} \tag{3}$$

where $c_i = 2\xi\omega_i m$ and $\Omega_i^2 = (\Delta t)^2 (k_i/m)$ are used to replace the expressions of m, c and k in Eq. (1). The left and right sides of Eq. (3) involve only the data at the end of the $(i-1)$th and ith time steps, respectively. After substituting Eq. (3) into the second line of Eq. (2), it becomes:

$$\begin{aligned} d_{i+1} = &\left[1 - (1-\alpha_2)\beta_3 \Omega_i^2\right] d_i \\ &+ [\beta_1 - (1-\alpha_2)\beta_3 2\xi\Omega_i] (\Delta t) v_i \\ &+ [\beta_2 - (1-\alpha_1)\beta_3] (\Delta t)^2 a_i \\ &+ (1-\alpha_2)\beta_3 F_i + p_{i+1} \end{aligned} \tag{4}$$

This equation only involves the ith time step data, and thus the second line of Eq. (2) reduces to a one-step difference equation. As a result, a family of one-step integration methods is achieved.

The next step is to appropriately determine the structure-dependent coefficients β_1 to β_3. At first, these coefficients are assumed to be functions of the time step and initial structural properties, i.e., $\Omega_0 = \omega_0(\Delta t)$ and $\omega_0 = \sqrt{k_0/m}$, where k_0 is an initial stiffness. This assumption is intended to avoid the recalculation of these coefficients during time integration. In addition, each of β_1 to β_3 is assumed to be a fractional of Ω_0, i.e., $\beta_i = N_i/D$, $i = 1, 2, 3$, and the order of Ω_0 for N_i must be less than that of D so that an unconditional stability can be obtained. This is because that an overshoot or even instability will experience in the response if the order of Ω_0 for N_i is equal to or larger than that of D. It is appropriate to assume that D is a quadratic polynomial function of Ω_0, which are learned from conventional implicit integration methods and can be expressed as:

$$D = (1-\alpha_1) + (1-\alpha_2)\gamma 2\xi\Omega_0 + (1-\alpha_2)\beta\sigma\Omega_0^2 \tag{5}$$

where the choice of $2\xi\Omega_0$ as a base of the linear polynomial term of Ω_0 is because it is related to c_0 since $c_0 = 2\xi\Omega_0 m/(\Delta t)$, and the choice of Ω_0^2 as a base of the quadratic polynomial term of Ω_0 is because it is related to k_0 since $\Omega_0^2 = (\Delta t)^2 (k_0/m)$. Besides, β and γ are undetermined scalar constants for governing the numerical properties. Notice that σ is a stability amplification factor, which can magnify an unconditional stability interval [39]. This choice of D is intended to have an unconditional stability and a second-order accuracy. On the other hand, $N_i = x_i + y_i 2\xi\Omega_0$, $i = 1, 2, 3$ can be taken, where N_i is assumed to be a linear polynomial function of Ω_0. Hence, the highest order of Ω_0 for N_i is only 1 and is less than that of D, which is 2. This assumption of β_i can achieve two goals. One is that the coefficient β_i will become a constant of $x_i/(1-\alpha_1)$ in the limit $\Omega_0 \to 0$ and the other is that it will tend to zero in the limit $\Omega_0 \to \infty$. Hence, for a small Ω_0 or a low-frequency mode, the assumed structure-dependent displacement difference equation will degenerate into a conventional displacement difference equation form while for a large Ω_0 or a high-frequency mode, the coefficient β_i approaches zero, which leads to $d_{i+1} \approx d_i$, and thus there will be no abnormal amplitude growth or even numerical instability in responses. As a result, the proposed family of methods can accurately integrate low-frequency modes as using a conventional integration method while no instability for high-frequency modes can be guaranteed because $d_{i+1} \approx d_i$ is found.

Convergence is a prerequisite for a numerical method. Hence, the assumed coefficients β_1 to β_3 must be determined to meet this requirement. A local truncation error can be used to determine an order of accuracy and thus the proof of consistency [22]. At the early development stage, a local truncation error is constructed from a free vibration response for determining the order of accuracy. Thus, zero dynamic loading is assumed for simplicity, which means $f_i = f_{i+1} = 0$ and thus $p_{i+1} = 0$. In addition, $\sigma = 1$ is also taken for simplifying the determinations of β_1 to β_3. The derivation of a local truncation error E for a structure-dependent integration method can be found in [35,36]. Using the local truncation error, β_1 to β_3 are appropriately determined so that the requirement of consistency

and thus a first-order accuracy are met. As a result, they are found to be:

$$\begin{aligned}\beta_1 &= \frac{1}{D}\left[(1-\alpha_1)+(1-\alpha_2)\,\gamma 2\xi\Omega_0\right]\\ \beta_2 &= \frac{\beta}{D}\frac{1-\alpha_1}{1-\alpha_2}+\frac{1}{D}\left[\frac{1}{2}(1-\alpha_1)\right.\\ &\quad\left.-\beta-(1-\alpha_2)\left(\beta-\frac{1}{2}\gamma\right)2\xi\Omega_0\right]\\ \beta_3 &= \frac{\beta}{D}\frac{1}{1-\alpha_2}\end{aligned} \tag{6}$$

After determining these coefficients, the corresponding local truncation error E can be used to reveal the order of accuracy of the proposed family of methods. As a result, it is simplified to be:

$$\begin{aligned}E = &-\frac{1}{D}\left(\alpha_1-\alpha_2+\gamma-\frac{1}{2}\right)\left[(\Delta t)\dddot{u}_i+\frac{1}{2}(\Delta t)^2\ddddot{u}_i\right]\\ &+\frac{1}{D}\beta\Omega_0^2\ddot{u}_i\\ &+\frac{1}{D}\left(\frac{1}{2}\gamma-\frac{1}{12}\right)2\xi\Omega_0(\Delta t)\dddot{u}_i\\ &+\frac{1}{D}\left(\alpha_2\gamma-\frac{1}{2}\alpha_2+\frac{1}{12}\right)(\Delta t)^2\ddddot{u}_i+O\left[(\Delta t)^3\right]\end{aligned} \tag{7}$$

A minimum order of accuracy 1 can be obtained and thus the consistency is verified for any α_1, α_2, β, γ and ξ. Besides, a second-order accuracy can be further yielded if $\alpha_1-\alpha_2+\gamma-\frac{1}{2}=0$ is met. Since a second-order accuracy is generally required for an integration method, the attention of this family of methods is restricted to the values of α_1, α_2 and γ for which $\alpha_1-\alpha_2+\gamma-\frac{1}{2}=0$ is satisfied in the subsequent study.

A stability amplification factor σ can be applied to multiply the terms related to Ω_0^2 in the displacement difference equation to magnify an unconditional stability interval. As a result, Eq. (5) is used to define the denominator of β_i. Based on this displacement difference equation, a loading term will be further determined. A local truncation error derived from a forced vibration case can be applied to determine the loading term. For this purpose, the local truncation error of the proposed family of methods, where σ, f_i, f_{i+1} and p_{i+1} are included in the formulation, is found to be:

$$\begin{aligned}E = &-\frac{1}{D}\left(\alpha_1-\alpha_2+\gamma-\frac{1}{2}\right)\left[(\Delta t)\dddot{u}_i+\frac{1}{2}(\Delta t)^2\ddddot{u}_i\right]\\ &+\frac{1}{D}\beta\Omega_0^2\ddot{u}_i+\frac{1}{D}\left(\frac{1}{2}\gamma-\frac{1}{12}\right)2\xi\Omega_0(\Delta t)\dddot{u}_i\\ &+\frac{1}{D}\left(\alpha_2\gamma-\frac{1}{2}\alpha_2+\frac{1}{12}\right)(\Delta t)^2\ddddot{u}_i\\ &+\frac{1}{BD}(1-\alpha_2)\,\beta\,(\sigma-1)\,2\xi\Omega_0\Omega_0\omega_0\dot{u}_i\\ &+\frac{1}{BD}(1-\alpha_2)\,\beta\,(\sigma-1)\left[1+(-\alpha_2\right.\\ &\left.+\gamma+\frac{1}{2}\right)2\xi\Omega_0\Big]\Omega_0^2\ddot{u}_i-\ddot{p}_{i+1}\\ &-\frac{1}{B}\left(p_{i+1}-p_i\right)-\frac{1}{B}2\xi\Omega_0 p_{i+1}\\ &+\frac{1}{B}(\alpha_2-\gamma)\,2\xi\Omega_0\left(p_{i+1}-p_i\right)\\ &-\frac{1}{BD}\alpha_2\beta\left[1-(\alpha_2-\gamma)\,2\xi\Omega_0\right]\frac{1}{m}(\Delta t)^2\ddot{f}_i\\ &+\frac{1}{BD}\beta\left[1-(2\alpha_2-\gamma)\,2\xi\Omega_0\right]\left[\frac{1}{m}(\Delta t)\dot{f}_i\right.\\ &\left.+\frac{1}{2}\frac{1}{m}(\Delta t)^2\ddot{f}_i\right]+\frac{1}{BD}\beta 2\xi\Omega_0\frac{1}{m}f_{i+1}\\ &+O\left[(\Delta t)^3\right]\end{aligned} \tag{8}$$

where $B=(1-\alpha_1)+(1-\alpha_2)\,\gamma 2\xi\Omega_0$. Apparently, this equation will reduce to Eq. (7) for the case of $\sigma=1$, $f_i=f_{i+1}=0$ and $p_{i+1}=0$. In general, the proposed family of methods can only possess a first-order accuracy for any combination of α_1, α_2, β, γ, ξ, σ and the dynamic loading of f_i as well as f_{i+1} in addition to $p_{i+1}=0$. It can be found that the satisfaction $\alpha_1-\alpha_2+\gamma-\frac{1}{2}=0$ is, in general, unable to have a second-order accuracy except for free vibration cases. It can be found that the term $\beta\Omega_0^2\ddot{u}_i/D$ will become a dominant error term for a large Ω_0 or a high-frequency mode as $\sigma=1$ and $\xi=0$ since it is the only quadratic and also the highest term of Ω_0. On the other hand, for the case of $\sigma\neq 1$ and $\xi\neq 0$, the error terms of $(1-\alpha_2)\,\beta\,(\sigma-1)\,2\xi\Omega_0\Omega_0\omega_0\dot{u}_i/BD$ and $(1-\alpha_2)\,\beta\,(\sigma-1)\left[1+\left(-\alpha_2+\gamma+\frac{1}{2}\right)2\xi\Omega_0\right]\Omega_0^2\ddot{u}_i/BD$ might also become significant. Consequently, it is very important to determine an appropriate loading term p_{i+1} to remove these error terms. As a result, the loading term is found to be:

$$p_{i+1}=\frac{1}{D}(1-\alpha_2)\,\beta\sigma\frac{1}{m}(\Delta t)^2\left(f_{i+1}-f_i\right) \tag{9}$$

After substituting this term into Eq. (8), it is largely simplified to be:

$$\begin{aligned}E = &-\frac{1}{D}\left(\alpha_1-\alpha_2+\gamma-\frac{1}{2}\right)\left[(\Delta t)\dddot{u}_i+\frac{1}{2}(\Delta t)^2\ddddot{u}_i\right]\\ &+\frac{1}{D}\left(\alpha_2\gamma-\beta-\frac{1}{2}\alpha_2+\frac{1}{12}\right)(\Delta t)^2\ddddot{u}_i\\ &-\frac{1}{D}\left(\beta-\frac{1}{2}\gamma+\frac{1}{12}\right)2\xi\Omega_0(\Delta t)\dddot{u}_i\end{aligned}$$

$$-\frac{1}{BD}(1-\alpha_2)\beta(\sigma-1)\left[(2\xi\Omega_0)^2\ddot{u}_i + 2(2\xi\Omega_0)(\Delta t)\dddot{u}_i + (\Delta t)^2\ddot{u}_i\right] + O\left[(\Delta t)^3\right] \quad (10)$$

Clearly, the local truncation error involves no loading terms and a second-order accuracy can be generally obtained only if $\alpha_1 - \alpha_2 + \gamma - \frac{1}{2} = 0$ is satisfied.

After determining the loading term p_{i+1} as shown in Eq. (9), the formulation of the proposed family of methods is completely yielded and it is a two-step integration method. It will reduce to the first Chang dissipative method [35] if $\alpha_1 = 0$ and $\alpha_2 = -\alpha$ are adopted. On the other hand, it will degenerate into the second Chang dissipative method [36] if $\alpha_1 = \alpha$ and $\alpha_2 = 0$ are chosen. The case of $\alpha_1 = \alpha_2 = 0$ can denote the non-dissipative Chang family method [30], where the member of $\beta = \gamma = \frac{1}{2}$ is the improved Chang explicit method [29] and the member of $\beta = \frac{1}{4}$ and $\gamma = \frac{1}{2}$ is the Chang explicit method [27]. Hence, most semi-explicit structure-dependent integration methods developed by Chang are covered by the proposed family of methods. For brevity, the proposed family of methods is referred as the Chang α-controlled method and is abbreviated as CAM herein. In general, the non-dissipative Chang family method is a one-step method, while the two Chang dissipative methods are two-step methods.

2.3 One-step method

A one-step method is generally preferred over a two-step method. Clearly, Eq. (2) is a two-step method and it can be converted to a one-step method if Eq. (4) is employed to replace the second line of Eq. (2). In Eq. (3), all the terms on the left side are the data at the $(i-1)$th time step, while those on the right side are the data at the ith time step. Thus, the use of the right side to replace the left side implies that the data at the $(i-1)$th time step, i.e., the terms of d_{i-1}, v_{i-1} and a_{i-1}, will disappear from the displacement difference equation as shown in Eq. (4). As a result, a family of one-step integration methods can be obtained and is:

$$\begin{aligned}
&(1-\alpha_1)ma_{i+1} + \alpha_1 ma_i + (1-\alpha_2)cv_{i+1} + \alpha_2 cv_i \\
&\quad + (1-\alpha_2)kd_{i+1} + \alpha_2 kd_i = (1-\alpha_2)f_{i+1} + \alpha_2 f_i \\
&d_{i+1} = d_i - \bar{\beta}_1\Omega_i^2 d_i + \bar{\beta}_2(\Delta t)v_i \\
&\quad - \bar{\beta}_1 2\xi\Omega_i(\Delta t)v_i + \bar{\beta}_3(\Delta t)^2 a_i + \bar{p}_{i+1} \\
&v_{i+1} = v_i + (\Delta t)\left[(1-\gamma)a_i + \gamma a_{i+1}\right]
\end{aligned} \quad (11)$$

where

$$\begin{aligned}
\bar{\beta}_1 &= (1-\alpha_2)\beta_3 = \frac{1}{D}\beta \\
\bar{\beta}_2 &= \beta_1 = \frac{1}{D}\left[(1-\alpha_1) + (1-\alpha_2)\gamma 2\xi\Omega_0\right] \\
\bar{\beta}_3 &= \beta_2 - (1-\alpha_1)\beta_3 = \frac{1}{D}\left\{\left[\frac{1}{2}(1-\alpha_1) - \beta\right]\right. \\
&\quad \left. - (1-\alpha_2)\left(\beta - \frac{1}{2}\gamma\right)2\xi\Omega_0\right\} \\
\bar{p}_{i+1} &= (1-\alpha_2)\beta_3 F_i + p_{i+1} \\
&= \frac{1}{mD}(1-\alpha_2)\beta\sigma(\Delta t)^2(f_{i+1} - f_i) \\
&\quad + \frac{1}{mD}\beta(\Delta t)^2 f_i
\end{aligned} \quad (12)$$

The coefficients $\bar{\beta}_1$ to $\bar{\beta}_3$ and $\bar{p}_{i+1}$ are functions of $\xi\Omega_0$ and Ω_0^2, which can be obtained after solving an eigenvalue problem. However, it will cost much time for solving an eigenvalue problem for a matrix of large order, and therefore, it is prohibited. There is an alternative way to avoid solving an eigenvalue problem by using $c_0 = 2\xi\omega_0 m$ and $\Omega_0^2 = (\Delta t)^2(k_0/m)$ to replace $\xi\Omega_0$ and Ω_0^2 in Eq. (12). As a result, it becomes:

$$\begin{aligned}
\bar{\beta}_1 &= \frac{1}{D}\beta m \\
\bar{\beta}_2 &= \frac{1}{D}\left[(1-\alpha_1)m + (1-\alpha_2)\gamma(\Delta t)c_0\right] \\
\bar{\beta}_3 &= \frac{1}{D}\left\{\left[\frac{1}{2}(1-\alpha_1) - \beta\right]m\right. \\
&\quad \left. - (1-\alpha_2)\left(\beta - \frac{1}{2}\gamma\right)(\Delta t)c_0\right\} \\
\bar{p}_{i+1} &= \frac{1}{D}(1-\alpha_2)\beta\sigma(\Delta t)^2(f_{i+1} - f_i) \\
&\quad + \frac{1}{D}\beta(\Delta t)^2 f_i
\end{aligned} \quad (13)$$

where $D = (1-\alpha_1)m + (1-\alpha_2)\gamma(\Delta t)c_0 + (1-\alpha_2)\beta\sigma(\Delta t)^2 k_0$. Apparently, the coefficients $\bar{\beta}_1$ to $\bar{\beta}_3$ and $\bar{p}_{i+1}$ are functions of the time step and initial structural properties, i.e., m, c_0 and k_0. Thus, they are structure dependent and will remain invariant for a complete step-by-step integration procedure.

3 Appropriate parameters

Because the numerical properties of CAM are dominated by parameters α_1, α_2, β and γ, it is needed to identify their limitations so that desired numerical

properties can be obtained. Notice that a stability analysis is generally required for the proof the convergence of an integration method. The application of CAM to calculate a forced vibration response for a linear elastic, single-degree-of-freedom system can be written in a recursive matrix form as:

$$\mathbf{X}_{i+1} = \mathbf{A}\mathbf{X}_i + \mathbf{L}\left[(1-\alpha_2)\, f_{i+1} + \alpha_2 f_i\right] \tag{14}$$

where $\mathbf{X}_{i+1} = \left[d_{i+1},\, (\Delta t) v_{i+1},\, (\Delta t)^2 a_{i+1}\right]^{\mathrm{T}}$ is defined; $\mathbf{A}$ is an amplification matrix and $\mathbf{L}$ is a load vector. The characteristic equation of the matrix $\mathbf{A}$ can be derived from $|\mathbf{A} - \lambda \mathbf{I}| = 0$ and is:

$$\lambda^3 - A_1\lambda^2 + A_2\lambda - A_3 = 0 \tag{15}$$

where λ is an eigenvalue of the matrix $\mathbf{A}$ and the coefficients A_1, A_2 and A_3 are found to be:

$$\begin{aligned}
A_1 &= 2 - \frac{1}{D}\left[\alpha_1 + (1-\alpha_2+\alpha_2\gamma)\, 2\xi\Omega_0 \right.\\
&\quad \left. + \left(\alpha_2\beta - \alpha_2\gamma - \frac{1}{2}\alpha_2 + \gamma + \frac{1}{2}\right)\Omega_0^2\right]\\
&\quad - \frac{1}{BD}\left[\alpha_1 + (1-\alpha_2+\alpha_2\gamma)\, 2\xi\Omega_0\right]\\
&\quad \times (1-\alpha_2)\,\beta\,(\sigma-1)\,\Omega_0^2\\
A_2 &= 1 - \frac{1}{D}\left[2\alpha_1 + (1-2\alpha_2+2\alpha_2\gamma)\, 2\xi\Omega_0 \right.\\
&\quad \left. + \left(2\alpha_2\beta - 2\alpha_2\gamma + \gamma - \frac{1}{2}\right)\Omega_0^2\right]\\
&\quad - \frac{1}{BD}\left[2\alpha_1 + (1-2\alpha_2+2\alpha_2\gamma)\, 2\xi\Omega_0\right]\\
&\quad \times (1-\alpha_2)\,\beta\,(\sigma-1)\,\Omega_0^2\\
A_3 &= -\frac{1}{D}\left[\alpha_1 - \alpha_2\,(1-\gamma)\, 2\xi\Omega_0 \right.\\
&\quad \left. + \alpha_2\left(\beta - \gamma + \frac{1}{2}\right)\Omega_0^2\right]\\
&\quad - \frac{1}{BD}\left[\alpha_1 - (1-\gamma)\,\alpha_2 2\xi\Omega_0\right]\\
&\quad \times (1-\alpha_2)\,\beta\,(\sigma-1)\,\Omega_0^2
\end{aligned} \tag{16}$$

Clearly, these coefficients will be largely reduced for the case of $\sigma = 1$.

It is complicated to analytically obtain the three eigenvalues of Eq. (15) for a general value of Ω_0 and σ. Therefore, to avoid the very complex algebraic manipulations, stability conditions for the limiting cases of $\Omega_0 \to 0$ and $\Omega_0 \to \infty$ in addition to $\sigma = 1$ are examined first. Although only the case of $\sigma = 1$ is considered, it will be shown later that the obtained results are applicable to a general value of σ. Both limiting cases can be applied to determine the limitations on α_1, α_2, β and γ for CAM. Notice that the three eigenvalues of the characteristic equation for a general Ω_0 can be numerically calculated. After obtaining the asymptotic values of the coefficients A_1, A_2 and A_3 in the limit $\Omega_0 \to 0$, the characteristic equation reduces to:

$$\left(\lambda + \frac{\alpha_1}{1-\alpha_1}\right)(\lambda - 1)^2 = 0 \tag{17}$$

The principal roots are $\lambda_{1,2} = 1$ and the spurious root is $\lambda_3 = -\alpha_1/(1-\alpha_1)$. Based on $|\lambda_3| \le 1$, an interval of $-\infty \le \alpha_1 \le 1/2$ is found. Besides, Eq. (15), in the limit $\Omega_0 \to \infty$, becomes:

$$\begin{aligned}
&\left(\lambda + \frac{\alpha_2}{1-\alpha_2}\right)\left[\lambda^2 - \left(2 - \frac{\gamma + \frac{1}{2}}{\beta}\right)\lambda \right.\\
&\quad \left. + \left(1 - \frac{\gamma - \frac{1}{2}}{\beta}\right)\right] = 0,
\end{aligned} \tag{18}$$

and its roots are found to be:

$$\begin{aligned}
\lambda_{1,2} &= 1 - \frac{\gamma + \frac{1}{2}}{2\beta} \pm \sqrt{\left(\frac{\gamma + \frac{1}{2}}{2\beta}\right)^2 - \frac{1}{\beta}},\\
\lambda_3 &= -\frac{\alpha_2}{1-\alpha_2}
\end{aligned} \tag{19}$$

where λ_3 only depends on α_2 and is independent of β and γ while $\lambda_{1,2}$ are functions of β and γ. A simple way can be used to determine the relationship between β and γ by assuming that the two principal eigenvalues are identical and real. As a result, it leads to:

$$\beta = \frac{1}{4}\left(\gamma + \frac{1}{2}\right)^2 = \frac{1}{4}(1 - \alpha_1 + \alpha_2)^2 \tag{20}$$

where $\gamma = 1/2 - \alpha_1 + \alpha_2$ is employed since it is required to have a second-order accuracy. Hence, the principal roots are found to be $\lambda_{1,2} = (-1 - \alpha_1 + \alpha_2)/(1 - \alpha_1 + \alpha_2)$ in addition to the spurious root of $\lambda_3 = -\alpha_2/(1-\alpha_2)$ after substituting β and γ into Eq. (19). These eigenvalues will be further applied to determine the parameters α_1 and α_2 next.

There is a great idea to simplify the stability conditions in the limit $\Omega_0 \to \infty$ by assuming that $|\lambda_{1,2}| = |\lambda_3| = \rho_\infty$, which implies that the characteristic equation of CAM possesses a triple root, and its absolute value is equal to the spectral radius in correspondence to $\Omega_0 \to \infty$. The spectral radius of an integration method is defined as $\rho = \max\left(|\lambda_1|, |\lambda_2|, |\lambda_3|\right)$ and the amount of numerical dissipation is closely related to its value. Clearly, ρ_∞ is a special case of ρ, which

is the spectral radius for a general value of Ω_0. As a result, the parameters α_1 and α_2 are found to be:

$$\alpha_1 = \frac{-1+2\rho_\infty}{1+\rho_\infty}, \quad \alpha_2 = \frac{\rho_\infty}{1+\rho_\infty} \tag{21}$$

where ρ_∞ can vary in the interval of $0 \le \rho_\infty \le 1$ so that the stability conditions can be met. This interval of ρ_∞ leads to $-1 \le \alpha_1 \le 1/2$, which is in the interval of $-\infty \le \alpha_1 \le 1/2$ that is required by the limiting case of $\Omega_0 \to 0$. Notice that ρ_∞ can provide a measure of numerical damping for high-frequency modes. This stability analysis in conjunction with the proof of consistency implies convergence. As a summary, CAM can have an unconditional stability, a second-order accuracy and a desired numerical damping if the following relationships are satisfied:

$$\beta = \frac{1}{4}(1-\alpha_1+\alpha_2)^2, \quad \gamma = \frac{1}{2} - \alpha_1 + \alpha_2 \tag{22}$$

where α_1 and α_2 are determined from Eq. (21). Clearly, CAM only has a free parameter ρ_∞.

4 Numerical properties

After applying the limiting cases of $\Omega_0 \to 0$ and $\Omega_0 \to \infty$ to determine the relationships for the parameters α_1, α_2, β and γ, it is of interest to assess the numerical properties of CAM for a general value of Ω_0. Because Eq. (15) with the coefficients given in Eq. (16) for the case of $\sigma = 1$ for CAM possesses exactly the same characteristic equation as that of the generalized-α method, the numerical properties of CAM with $\sigma = 1$ for one-step and two-step methods for linear elastic systems will be the same as those of the generalized-α method, such as stability conditions, relative period error, and numerical damping if these properties are derived from the same characteristic equation. Consequently, there is no need to re-evaluate the basic numerical properties of CAM for linear elastic systems. However, the analytical results are summarized for brevity. In addition, the other properties will be thoroughly explored for both linear elastic and nonlinear systems, such as stability, overshoot and weak instability.

4.1 Basic numerical properties

The basic numerical properties of CAM with $\sigma = 1$, such as the spectral radius, relative period error and numerical damping, are summarized in Fig. 1. The variation of the spectral radius versus $\Delta t/T_0$ for different ρ_∞ is shown in Fig. 1a. It is revealed by each curve that the spectral radius ρ tends to become the same as ρ_∞ when $\Delta t/T_0$ is large enough, say 1000. It is also seen that the spectral radius goes down from 1 to ρ_∞ for each curve as Ω_0 goes up from zero to infinity. As a result, CAM is unconditionally stable for linear elastic systems. This fact in conjunction with consistency implies the convergence of CAM. Figure 1b shows variations of relative period error versus $\Delta t/T_0$, while variations of numerical damping ratio versus $\Delta t/T_0$ is displayed in Fig. 1c. In Fig. 1b, the curve of $\rho_\infty = 1.0$ has the smallest relative period error. In general, the relative period error rises with the decrease of ρ_∞ for a given $\Delta t/T_0$. The curve for $\rho_\infty = 1.0$ has zero numerical damping as shown in Fig. 1c. On the other hand, the rest curves can possess a favorable numerical damping. In fact, each curve has a zero tangent at the origin and subsequently a controlled turn upward. Hence, CAM can have adequate high-frequency numerical damping while the low-frequency responses are not affected too strongly. In addition, the closer the value of ρ_∞ approaching zero, the larger the numerical damping and period distortion.

4.2 Improved stability by σ

To improve stability property for CAM, a stability amplification factor σ is adopted to adjust the displacement difference equation. Although a slight modification is made for the displacement difference equation, it might alter the numerical properties of CAM. As a result, both the linear and nonlinear performances of CAM with σ should be further evaluated. For a nonlinear system, the stiffness might vary per time step and thus the amplification matrix varies accordingly. Thus, the amplification matrix $\mathbf{A}$ in Eq. (15) must be replaced by $\mathbf{A}_{i+1}$, which is introduced to represent the amplification matrix at the end of the $(i+1)$th time step. Hence, $\mathbf{A}_{i+1} = [A_{mn}]$, $m, n = 1, 2, 3$. The explicit expressions of A_{mn} are found to be:

$$A_{11} = \left(1 - \bar{\beta}_1 \Omega_i^2\right) \quad A_{12} = \bar{\beta}_2 - \bar{\beta}_1 2\xi\Omega_i \quad A_{13} = \bar{\beta}_3$$

$$A_{21} = -\frac{\gamma}{B}\left[\Omega_{i+1}^2 + (1-\alpha_2)\,\bar{\beta}_1 \Omega_i^2 \Omega_{i+1}^2\right]$$

$$A_{22} = 1 - \frac{\gamma}{B}\left[2\xi\Omega_{i+1} + (1-\alpha_2)\left(\bar{\beta}_2 - \bar{\beta}_1 2\xi\Omega_i\right)\Omega_{i+1}^2\right]$$

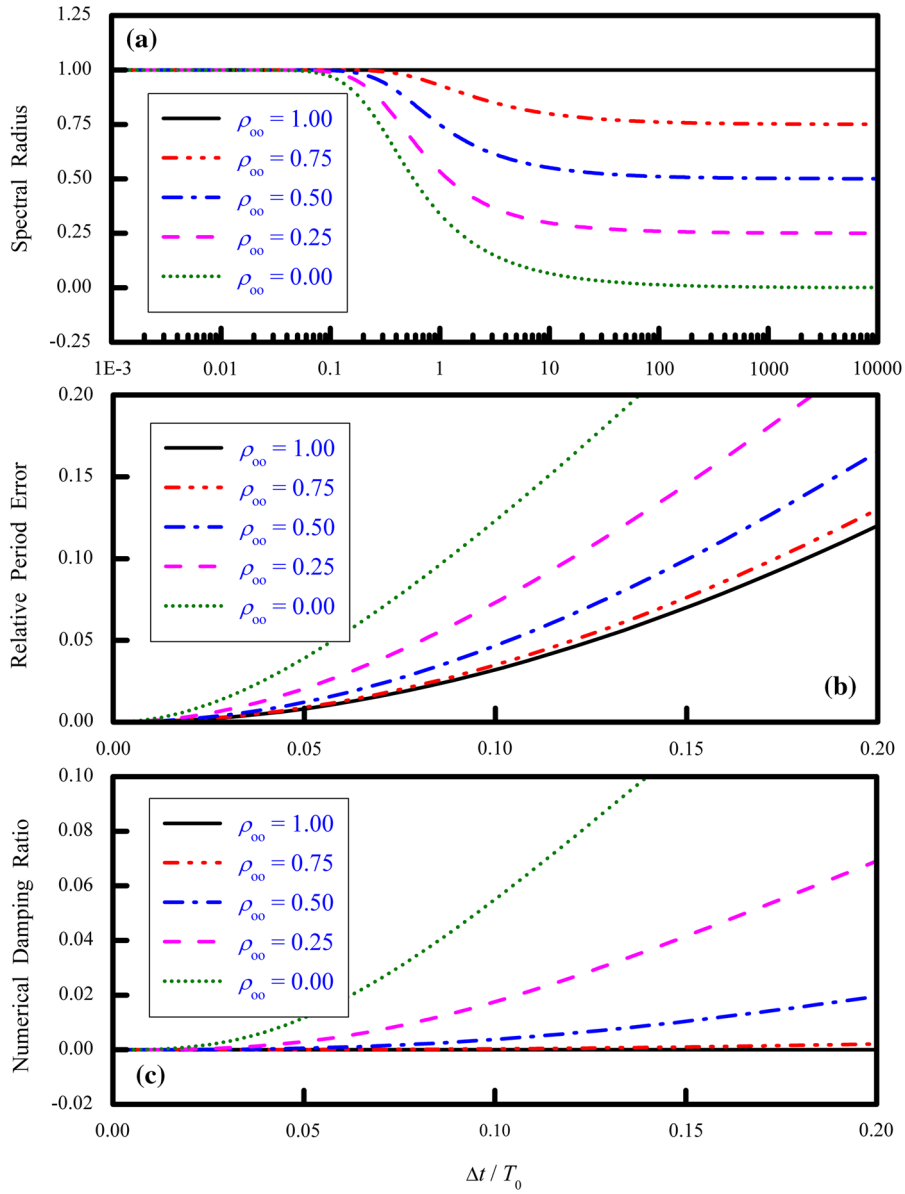

Fig. 1 Numerical properties for linear elastic systems

$$
\begin{aligned}
A_{23} &= 1-\gamma-\frac{\gamma}{B}\{\alpha_1+(1-\alpha_2)\\
&\quad\times\left[(1-\gamma)\,2\xi\Omega_0+\bar{\beta}_3\Omega_{i+1}^2\right]\}\\
A_{31} &= -\frac{1}{B}\left[\Omega_{i+1}^2+(1-\alpha_2)\,\bar{\beta}_1\Omega_i^2\Omega_{i+1}^2\right]\\
A_{32} &= -\frac{1}{B}\left[2\xi\Omega_{i+1}+(1-\alpha_2)\left(\bar{\beta}_2-\bar{\beta}_1 2\xi\Omega_i\right)\Omega_{i+1}^2\right]\\
A_{33} &= -\frac{1}{B}\{\alpha_1+(1-\alpha_2)\\
&\quad\times\left[(1-\gamma)\,2\xi\Omega_{i+1}+\bar{\beta}_3\Omega_{i+1}^2\right]\}
\end{aligned}
\tag{23}
$$

where $B=(1-\alpha_1)+(1-\alpha_2)\,\gamma 2\xi\Omega_0$. In addition, the relations of $\Omega_i^2=\delta_i\Omega_0^2$ and $\Omega_{i+1}^2=\delta_{i+1}\Omega_0^2$ can be found from the definitions of δ_i and δ_{i+1}. Similarly, the characteristic equation of the matrix $\mathbf{A}_{i+1}$ at the end of the $(i+1)$th time step can be obtained from $|\mathbf{A}_{i+1}-\lambda\mathbf{I}|=0$ and will have the same form as shown in Eq. (15), where A_1 = trace of $\mathbf{A}_{i+1}$; A_2 = sum of principal minors of $\mathbf{A}_{i+1}$ and A_3 = determinant of $\mathbf{A}_{i+1}$. Although it is complicated to derive the mathematical expressions of A_1, A_2 and A_3 for evaluating the numerical properties of CAM, it can be done numer-

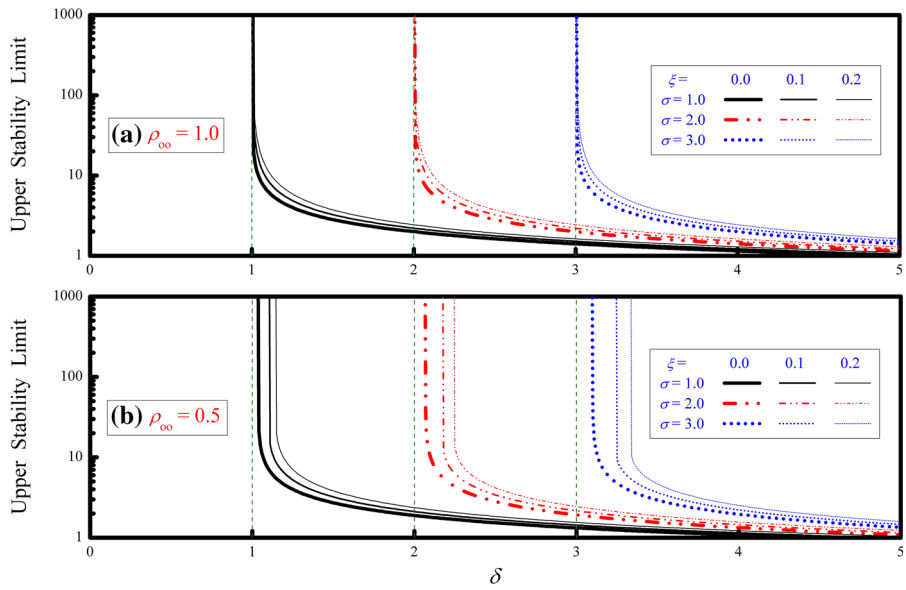

Fig. 2 Variation of upper stability limit with δ_{i+1} for CAM

ically. Notice that the assessments of CAM for nonlinear systems are conducted only for a specific time step but not for a whole integration procedure due to the variation of stiffness. However, the results are still indicative since a whole integration procedure consists of each time step.

Using the characteristic equation of $\mathbf{A}_{i+1}$, the three eigenvalues of CAM can be obtained for given ξ, δ_i and δ_{i+1} for a specific Ω_0, which will start from a very small to very large values. The upper stability limit $\Omega_0^{(u)}$ is the maximum value of Ω_0, whose spectral radius is less than or equal to 1. A variety of nonlinear cases will be simulated by the combinations of δ_i and δ_{i+1} in the subsequent study. However, $\delta_i = \delta_{i+1} = \delta$ is generally assumed for brevity, since δ_{i+1} is close to δ_i for the consecutive time steps. To substantiate that σ can enlarge an unconditional stability interval, the variations of $\Omega_0^{(u)}$ versus δ are shown in Fig. 2 for CAM with $\rho_\infty = 1.0$ and 0.5. A part of the curve disappears in each plot and this part is corresponding to an infinite upper stability limit. An unconditional stability interval of $\delta \leq \sigma$ is found for CAM with $\rho_\infty = 1.0$, while it will become conditionally stable in the interval of $\delta > \sigma$ for different $\xi = 0$, 0.1 and 0.2. Clearly, $\sigma = 1$ implies that the stability amplification factor is not applied to CAM, and thus the curves in Fig. 2a reveal that CAM can have an unconditional stability interval of $\delta \leq 1$ and a conditional stability interval of $\delta > 1$. Whereas, an unconditional stability interval is extended from $\delta \leq 1$ to $\delta \leq 2$ for $\sigma = 2$ and to $\delta \leq 3$ for $\sigma = 3$. It is also found that the upper stability limit will rise with increasing δ in the conditionally stable interval. A very similar phenomenon is also seen in Fig. 2b as $\rho_\infty = 0.5$. However, it seems that σ can enlarge the unconditional stability interval to be slightly larger than that of $\delta \leq \sigma$ for $\rho_\infty = 0.5$. In fact, it can be expressed as $\delta \leq \bar{\sigma}$, where $\bar{\sigma} \geq \sigma$. It is evident from Fig. 2 that σ can alter the unconditional stability interval from $\delta \leq 1$ to $\delta \leq \sigma$. Clearly, a large σ will lead to a large unconditional stability interval and thus a stability amplification factor is also applicable to CAM. There is no need to choose $\sigma > 2$ since for a real structure its instantaneous stiffness is rare to become larger than twice of that of the initial stiffness. As a result, the case of $\delta \leq 2$ is considered herein since this interval is large enough for practical interest.

A two-degree-of-freedom spring–mass system is applied to numerically confirm the stability properties of CAM and the effectiveness of the stability amplification factor. The spring constant in correspondence to each lumped mass is assumed to be:

$$k = k_0 \left[1 + \varepsilon \sqrt{|\Delta u|}\right] \tag{24}$$

where k_0 is the initial spring constant; Δu is the amount of elongation of the spring and ε is a given constant. The lumped mass of each degree of freedom is taken as $m_1 = m_2 = 1kg$. Equation (24) is employed to simulate three different stiffness types of systems S1 to S3 if ε is appropriately chosen.

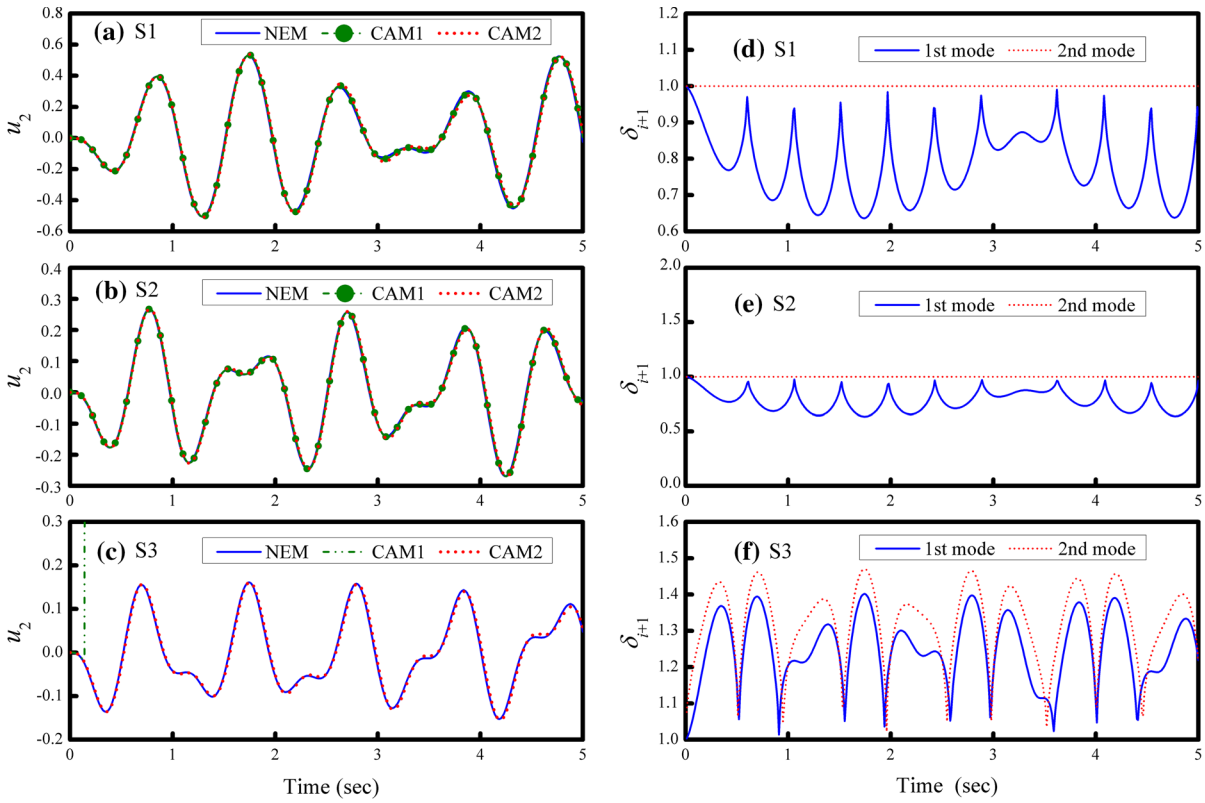

Fig. 3 Responses to three 2-DOF systems with different stiffness types

$$\begin{aligned} &\text{S1}: \varepsilon_1 = -0.1, \varepsilon_2 = -0.5 \quad \text{stiffness softening} \\ &\text{S2}: \varepsilon_1 = 0, \varepsilon_2 = 0 \quad \text{linear elastic} \\ &\text{S3}: \varepsilon_1 = 10^3, \varepsilon_2 = 1.0 \quad \text{stiffness hardening} \end{aligned} \tag{25}$$

where ε_1 and ε_2 are the constants for the first and second lumped masses, respectively. Besides, the initial spring constants for the first and second lumped masses are taken as $k_0 = 10^8$ N/m and $k_0 = 10^2$ N/m, respectively. As a result, the initial natural frequencies of the system are found to be 10 and 10^4 rad/s. The system is excited by a sinusoidal acceleration of $10\sin(2\pi t)$ at its base.

In the subsequent study, CAM with $\rho_\infty = 0.5$ and $\sigma = 1$ is referred as CAM1 while that with $\rho_\infty = 0.5$ and $\sigma = 2$ is referred as CAM2 for brevity. Both CAM1 and CAM2 can have desired numerical damping, where CAM1 possesses an unconditional stability interval of $\delta_{i+1} \leq 1$ while for CAM2, it has $\delta_{i+1} \leq 2$. Both methods with $\Delta t = 0.01$ s are applied to calculate the responses. In addition, the result obtained from the Newmark explicit method (NEM) [2] with $\Delta t = 0.0001$ s is considered as a reference solution. The calculated results of u_2, which is the displacement response at the second degree of freedom, are shown in Fig. 3a–c. In addition, the time histories of δ_{i+1} for both modes are shown in Fig. 3d–f. It is manifested from Fig. 3a–c that CAM1 can provide reliable solutions for S1 and S2, while for S3, it leads to instability very rapidly, whereas CAM2 can give accurate solutions for all the three systems. This can be explained next. Figure 3d shows that δ_{i+1} is close to 1 for the second mode of S1 while it varies between about 0.6 and 1.0 for the first mode. Clearly, δ_{i+1} is always equal to 1 for both modes of S2 since it is a linear elastic system. It can be seen in Fig. 3f for S3 that δ_{i+1} roughly varies in the intervals of $1 \leq \delta_{i+1} \leq 1.4$ and $1 \leq \delta_{i+1} \leq 1.5$ for the first and second modes, respectively. Because CAM1 can only possess an unconditional stability interval of $\delta_{i+1} \leq 1$ it can give reliable solutions for S1 and S2. Whereas, it becomes conditionally stable in the interval of $\delta_{i+1} > 1$. Hence, the violation of the upper stability limit is responsible for the instability occurred in S3 for using CAM1. In fact, it can be found from Fig. 2b that the upper stability limit $\Omega_0^{(u)}$ is only about 2.7 as $\delta_{i+1} = 1.5$ while the Ω_0 value for the second

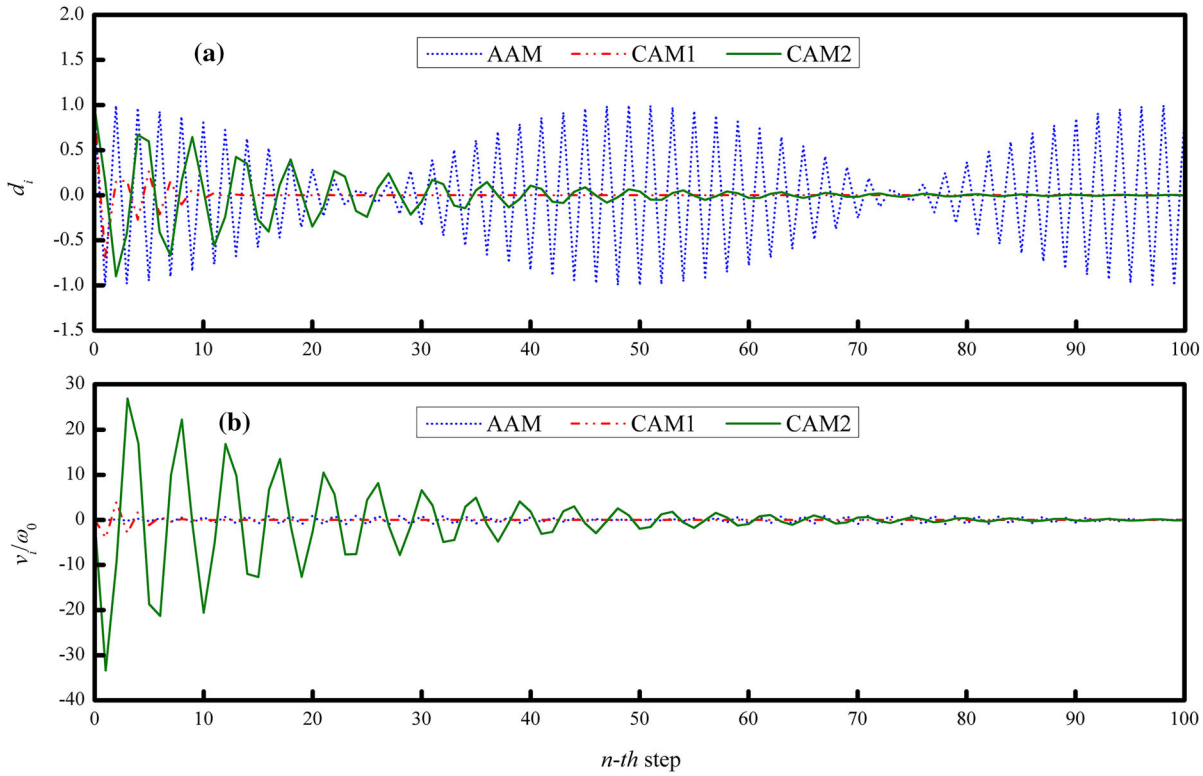

Fig. 4 Overshooting behavior of CAM in transient response

mode is found to be as large as $\Omega_0 = \omega_0(\Delta t) = 10^2$, which is much larger than $\Omega_0^{(u)} = 2.7$. In contrast, CAM2 can have an unconditional stability interval of $0 < \delta_{i+1} \leq 2$, and thus, it can give reliable solutions for the three systems, where δ_{i+1} varies within the interval of $0 < \delta_{i+1} \leq 1.5$.

Two important analytical results are thoroughly confirmed by this numerical example. One is that CAM with $\sigma = 1$ only has an unconditional stability for linear elastic and stiffness softening systems, i.e., $0 < \delta_{i+1} \leq 1$, while it becomes conditionally stable for stiffness hardening systems, i.e., $\delta_{i+1} > 1$, and the other is that a stability amplification factor can enlarge the unconditional stability interval from $0 < \delta_{i+1} \leq 1$ to $0 < \delta_{i+1} \leq 2$ if $\sigma = 2$ is adopted.

4.3 Overshoot

A general structure-dependent integration method might experience two types of overshoot although it can have an unconditional stability. One is in high-frequency transient responses and the other is in high-frequency steady-state responses. Since an overshoot might result in an inaccurate solution, it must be thoroughly explored for an integration method.

4.3.1 Overshoot in transient response

A high-frequency overshoot in transient response has been found by Goudreau and Taylor [41] although the integration method is unconditionally stable. A technique has been proposed by Hilber and Hughes [42] to detect such an overshoot. To assess the overshoot potential of an integration method, one can compute the discrete displacement and velocity in terms of the previous step data. In general, these results as $\Omega_0 \to \infty$ can give an indication of the high-frequency behavior of the integration method. Using Eq. (14), the following equations can be obtained in the limit $\Omega_0 \to \infty$.

$$d_{i+1} = \left[1 - \frac{\frac{1}{2}(1-\alpha_1)}{(1-\alpha_2)\beta\sigma}\right] d_i,$$
$$v_{i+1} = \left(\frac{\gamma}{2\beta\sigma} - 1\right)\Omega_0\omega_0 d_i + \left(1 - \frac{\gamma}{\beta\sigma}\right) v_i \qquad (26)$$

There is no overshoot in displacement for any member of CAM, while it generally shows a tendency to overshoot linearly in Ω_0 in the velocity equation.

The free vibration response of a single-degree-of-freedom system for the initial conditions of $d_0 = 1$ and $v_0 = 0$ can be employed to confirm the overshooting behavior of CAM. A time step of $\Delta t = 10T_0$ is chosen for each time history analysis and the results are plotted in Fig. 4. The constant average acceleration method (AAM) is also used to solve the same problem and the results are also shown in the figure for comparison. The velocity term is divided by the initial natural frequency of the system so that it can have the same unit as displacement. There is no overshoot in displacement for both CAM1 and CAM2 in Fig. 4 while an overshoot in velocity is found. These overshooting behaviors both in displacement and velocity for CAM1 and CAM2 are highly consistent with the analytical predictions shown in Eq. (26).

4.3.2 Overshoot in steady-state response

A high-frequency overshoot in steady-state responses has been found for a structure-dependent method [40] although it has never been seen for a conventional integration method. The root cause of this overshoot is due to the lack of a loading term in the displacement difference equation, i.e., $\bar{p}_{i+1}$ in Eq. (11) [40]. A numerical example is used to illustrate the importance of using the loading term $\bar{p}_{i+1}$ to remove this type of overshoot for CAM. Thus, a forced vibration response to a linear elastic, single-degree-of-freedom system is considered. The equation of motion can be written as:

$$m\ddot{u} + k_0 u = k_0 \sin(\bar{\omega} t) \tag{27}$$

where $\bar{\omega}$ is a driving frequency. An exact solution of this equation for zero initial conditions can be theoretically obtained and is:

$$u(t) = -\frac{w}{1-w^2}\sin(\omega t) + \frac{1}{1-w^2}\sin(\bar{\omega} t) \tag{28}$$

where $w = \bar{\omega}/\omega_0$ is a frequency ratio. On the right side of this equation, the first and second terms are a transient and steady-state responses, respectively. Thus, for a high-frequency mode or a large ω_0, the ratio w will tend to zero. As a result, Eq. (28) will reduce to $u(t) \approx \sin(\bar{\omega} t)$. This implies that the total response is almost dominated by the steady-state response and the transient response contributes insignificantly. Hence, a forced vibration response of a high-frequency system can be applied to reveal an adverse overshoot behavior in high-frequency steady-state responses.

A high-frequency system is mimicked by choosing $m = 1\,\text{kg}$ and $k_0 = 10^8\,\text{N/m}$. Hence, the natural frequency of the system is 10^4 rad/s. In addition, a driving frequency of $\bar{\omega} = 1$ rad/s is adopted. Thus, $w = 10^{-4}$ is found. Clearly, an accurate solution can be achieved if the steady-state response is reliably obtained. It has been shown [43] that a harmonic load can be faithfully captured if $\Delta t/\bar{T}$ is less than *1/12*, where $\bar{T}$ is the period of the applied harmonic load. Thus, $\Delta t = 0.5$ s is capable to accurately integrate the steady-state response since the value of $\Delta t/\bar{T}$ is as small as $1/(4\pi)$, where $\bar{T} = 2\pi/\bar{\omega} = 2\pi$. Both CAM1 and CAM2 without and with $\bar{p}_{i+1}$ are employed to calculate the forced vibration responses and the calculated results are plotted in Fig. 5. The results obtained from CAM1 and CAM2 without $\bar{p}_{i+1}$ are shown in Fig. 5a, b, respectively; and they exhibit a high-frequency overshoot in the steady-state responses. On the other hand, the results calculated by using CAM1 and CAM2 with $\bar{p}_{i+1}$ are shown in Fig. 5c, d, respectively, where the results overlap the exact solution. Apparently, CAM without a loading term will lead to a high-frequency overshoot in the steady-state response, while this undesirable overshoot can be taken out by adjusting the displacement difference equation with an appropriate loading term $\bar{p}_{i+1}$. Hence, this loading term must be included in the formulation of CAM.

5 No weak instability

A weak instability property has been found for some structure-dependent integration methods, such as the CR method, KR method and the method proposed by Tang and Lou. Both analytical and numerical methods have been applied to explore the weak instability property and can be found in [37,38,44,45]. A weak instability may lead to an inaccurate solution or even instability although an appropriate time step is used. Thus, it is important to explore whether CAM has such an undesirable weak instability. A technique has been used to assess this adverse property by analytically deriving a free vibration response of a linear elastic, single-degree-of-freedom system [38,44,45].

Apparently, the application of CAM to analytically obtain the free vibration response of an undamped, linear elastic single-degree-of-freedom system can be

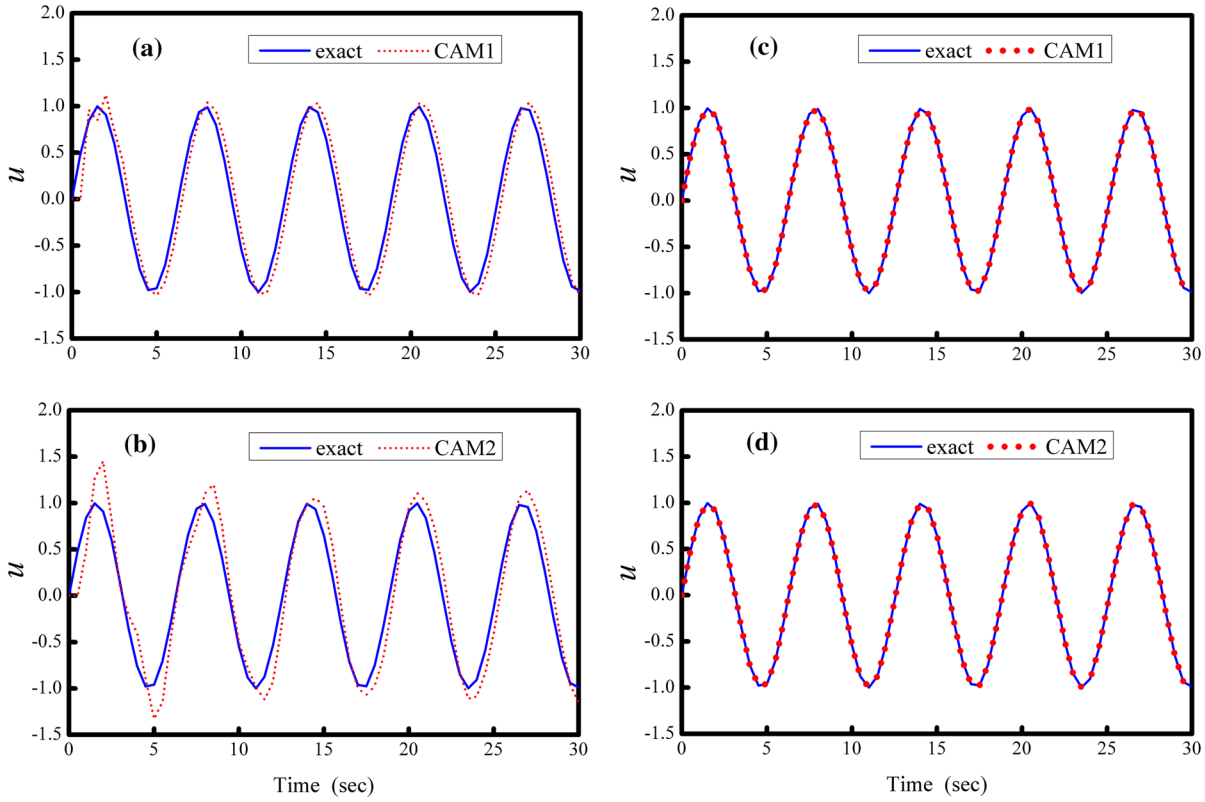

Fig. 5 Steady-state response to sine load for CAM1 and CAM2

applied to disclose whether CAM has a weak instability property or not. Hence, the equation of motion as shown in Eq. (1) can be solved for this purpose. For simplicity, zero viscous damping and zero dynamic loading are taken. In addition, the initial conditions of the initial displacement of d_0 and initial velocity of v_0 are assumed. The free vibration response can be analytically obtained from structural dynamics theory and is found to be:

$$d_n = \cos(n\Omega_0)\, d_0 + \frac{\sin(n\Omega_0)}{\Omega_0}(\Delta t)\, v_0 \tag{29}$$

where $d_n = u(t_n)$ and $t_n = n(\Delta t)$. On the other hand, CAM is also used to solve the same problem. This integration procedure is analytically conducted but not actually calculated by a computer. As a result, the complete solution procedure for CAM can be also expressed as shown in Eq. (14). Thus, after repeated substitutions for the case of zero dynamic loading, it reduces to:

$$\mathbf{X}_n = \mathbf{A}^n \mathbf{X}_0 \tag{30}$$

where $\mathbf{X}_0 = \left[d_0,\ (\Delta t)\, v_0,\ (\Delta t)^2 a_0 \right]^{\mathrm{T}}$. The initial acceleration a_0 can be determined from the equation of motion for the initial values of d_0 and v_0 and is found to be $(\Delta t)^2 a_0 = -\Omega_0^2 d_0$ for zero viscous damping.

It is very hard to analytically derive the numerical solution for using CAM for a general Ω_0 due to the very complex characteristic equation. As an alternative, the limiting case of $\Omega_0 \to \infty$ is considered since it can disclose high-frequency behaviors. In this case, the characteristic equation of CAM has a triple root of $\lambda_{1,2,3} = -\rho_\infty$ and has no three linearly independent eigenvectors. Hence, the matrix $\mathbf{A}$ is not diagonalizable and is unable to obtain $\mathbf{A} = \mathbf{\Phi}\mathbf{\Lambda}^n\mathbf{\Phi}^{-1}$, where $\mathbf{\Lambda}$ is a diagonal matrix and its diagonal terms are λ_i, $i = 1, 2, 3$; and $\mathbf{\Phi}$ is the corresponding eigenvector matrix. However, it is possible to convert the matrix $\mathbf{A}$ to a Jordan canonical form, such as $\mathbf{A} = \mathbf{\Psi}\mathbf{J}\mathbf{\Psi}^{-1}$, through a non-singular matrix $\mathbf{\Psi}$. Notice that $\mathbf{J}$ is the Jordan form of the matrix $\mathbf{A}$. As a result, Eq. (30) is rewritten as:

$$\mathbf{X}_n = \mathbf{A}^n \mathbf{X}_0 = \mathbf{\Psi}\mathbf{J}^n\mathbf{\Psi}^{-1}\mathbf{X}_0 \tag{31}$$

where the eigenvector matrix is $\mathbf{\Psi} = \left[\psi_1\ \psi_2\ \psi_3 \right]$; and the eigenvectors of ψ_1, ψ_2 and ψ_3 can be determined

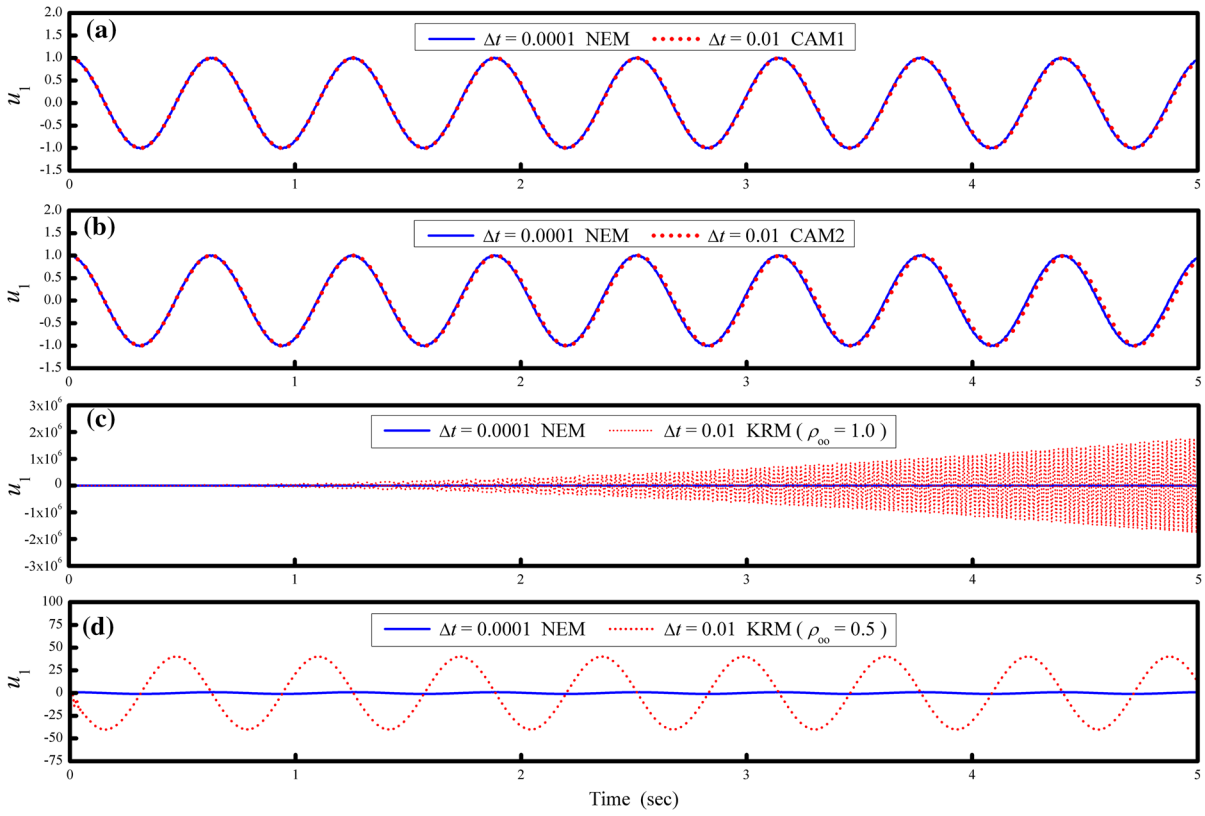

Fig. 6 Free vibration responses to 2-story shear-beam-type building

from $(\mathbf{A}-\lambda)\psi_1 = 0$, $(\mathbf{A}-\lambda)\psi_2 = \psi_1$ and $(\mathbf{A}-\lambda)\psi_3 = \psi_2$, respectively. In addition, the matrices of $\mathbf{J}$ and $\mathbf{J}^n$ are found to be:

$$\mathbf{J} = \begin{bmatrix} \lambda & 1 & 0 \\ 0 & \lambda & 1 \\ 0 & 0 & \lambda \end{bmatrix}, \quad \mathbf{J}^n = \begin{bmatrix} \lambda^n & n\lambda^{n-1} & n\,(n-1)\,\lambda^{n-2} \\ 0 & \lambda^n & n\lambda^{n-1} \\ 0 & 0 & \lambda^n \end{bmatrix} \tag{32}$$

for a triple root λ. Consequently, Eq. (31) is applied to analytically derive the numerical solution in a mathematical form in correspondence to Eq. (29). As a result, the numerical solution for CAM is found to be:

$$d_n = (-\rho_\infty)^n\, d_0 \tag{33}$$

For comparison, the result for KRM has been found in [38] and is also listed below for comparison.

$$\begin{aligned} d_n = &-[(n+1)\,\rho_\infty + n]\,(-\rho_\infty)^{n-1}\, d_0 \\ &+n\,(-\rho_\infty)^{n-1}\,(\Delta t)\, v_0 \end{aligned} \tag{34}$$

In Eq. (29), the coefficient of d_0 is $\cos(n\Omega_0)$, which is bounded in $[-1,\ 1]$; and that for $(\Delta t)\, v_0$ is $\sin(n\Omega_0)/\Omega_0$, which is bounded in [0, 1]. In Eq. (33), the coefficient of d_0 is equal to $(-\rho_\infty)^n$, which is always less than or equal to 1; and there exists no $(\Delta t)\, v_0$ term. It is evident that there is no weak instability for CAM. Unlike the coefficient shown in Eq. (33), the coefficients of d_0 and $(\Delta t)\, v_0$ in Eq. (34) for KRM increase with the increase in n although they will diminish to zero as $|\rho_\infty| < 1$ after a period of time. This indicates that d_n will increase with increase in n in the early response although it might reduce to zero for $|\rho_\infty| < 1$. The growth of d_n is a linear function of n. A weak instability is, in general, applicable to polynomial growth in n of arbitrary order. This type of growth is less significant than that of the instability caused by a spectral radius greater than 1. It is evident that KRM has a weak instability, while CAM has no such an adverse property.

To confirm that CAM has no weak instability, a linear elastic 2-story shear-beam-type building is considered. The equation of motion is simply expressed as:

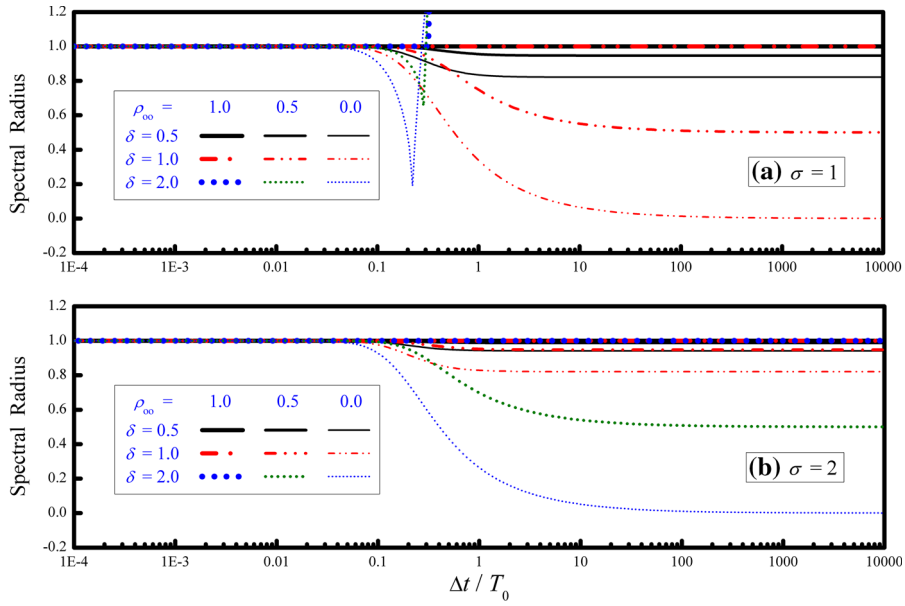

Fig. 7 Variation of spectral radius with $\Delta t/T_0$ for different ρ_∞ and δ values

$$\begin{bmatrix} 10^4 & 0 \\ 0 & 10^4 \end{bmatrix} \begin{Bmatrix} \ddot{u}_1 \\ \ddot{u}_2 \end{Bmatrix} + \begin{bmatrix} 5\times 10^{17} + 2\times 10^6 & -5\times 10^{17} \\ -5\times 10^{17} & 5\times 10^{17} \end{bmatrix} \begin{Bmatrix} u_1 \\ u_2 \end{Bmatrix} = \begin{Bmatrix} 0 \\ 0 \end{Bmatrix} \tag{35}$$

The natural frequencies of the system are found to be $\omega_1 = 10$ and $\omega_2 = 10^7$ rad/s; and its modal shapes are found to be:

$$\phi_1 = \begin{Bmatrix} 1 \\ 1 \end{Bmatrix}, \quad \phi_2 = \begin{Bmatrix} 1 \\ -1 \end{Bmatrix} \tag{36}$$

An initial displacement vector $\mathbf{u}_0$ is made up of both modes and is defined as:

$$\mathbf{u}_0 = \begin{Bmatrix} u_1(0) \\ u_2(0) \end{Bmatrix} = \phi_1 + \frac{1}{100}\phi_2 = \begin{Bmatrix} 1.01 \\ 0.99 \end{Bmatrix} \tag{37}$$

The free vibration responses to $\mathbf{u}_0$ with a zero-velocity vector are calculated by using CAM1 and CAM2 with $\Delta t = 0.01$ s. In addition, KRM with $\rho_\infty = 1.0$ and 0.5 is also applied to compute the response for comparison. The result calculated from NEM with $\Delta t = 0.0001$ s is considered as a reference solution. The responses of u_1 are shown in Fig. 6. It is revealed by Fig. 6a, b that CAM1 and CAM2 give reliable results although an initial displacement vector includes a high-frequency mode. However, the results obtained from KRM either with $\rho_\infty = 1.0$ or 0.5 shows a very significant amplitude growth due to a weak instability as shown in Fig. 6c, d. It is evident that the amplitude growth effect for KRM with $\rho_\infty = 1.0$ is much greater than that of KRM with $\rho_\infty = 0.5$. This may be because that the latter can have a high-frequency numerical damping to repress the high-frequency response. However, it is very important to note that an amplitude growth due to a weak instability still appears and it cannot be taken out by numerical damping.

6 Nonlinear performance

Although CAM has been explored for linear elastic systems, it is important to further study its nonlinear performance. The analysis of a nonlinear system is based on the von Neuman assumption of a solution in exponential form. Notice that the analysis is performed only for the $(i+1)$th time step but not for a whole integration procedure. However, it can still give useful predictions because an integration procedure consists of each time step. In general, the cases of $\delta_i = \delta_{i+1} = \delta = 0.5$, 1.0, and 2.0 will be calculated so that the three different stiffness types of softening, linear elastic, and hardening can be simulated.

6.1 Stability

Figure 7 shows the variation of spectral radius versus $\Delta t/T_0$. In Fig. 7a, the spectral radius ρ is less than or equal to 1 as $\delta \leq 1$ and finally tends to a certain constant smaller than 1, while it will become greater

than 1 after a certain value of $\Delta t/T_0$ as $\delta > 1$. This implies that CAM can have an unconditional stability interval of $\delta \leq 1$, and it becomes conditionally stable in the interval $\delta > 1$ if $\sigma = 1$ is adopted. Whereas, the spectral radius is always less than or equal to 1 as $\delta \leq 2$ shown in Fig. 7b. This is consistent with the analytical result that the application of the stability amplification factor σ to CAM can effectively enlarge the unconditional stability interval from $\delta_{i+1} \leq 1$ to $\delta_{i+1} \leq \sigma$. In general, each curve has a unit spectral radius for small $\Delta t/T_0$, while it goes down step by step and finally tends to a certain constant smaller than 1. For given δ and $\Delta t/T_0$, the spectral radius will decrease with the decrease of ρ_∞, whereas for given ρ_∞ and $\Delta t/T_0$, it will decrease with the increase of δ.

6.2 Period distortion and numerical dissipation

A bounded oscillatory response can be obtained from an integration method if its two principal eigenvalues $\lambda_{1,2}$ are complex conjugates in addition to $|\lambda_{1,2}| \leq 1$. Thus, the numerical properties of CAM at the $(i+1)$th time step can be assessed after writing the complex conjugate eigenvalues of the matrix $\mathbf{A}_{i+1}$ in an exponential form as:

$$\lambda_{1,2} = a \pm jb = e^{-\bar{\xi}\bar{\Omega}_{i+1} \pm j\bar{\Omega}^D_{i+1}} \tag{38}$$

where $j = \sqrt{-1}$, $\bar{\Omega}_{i+1} = \bar{\omega}_{i+1}(\Delta t)$ and $\bar{\Omega}^D_{i+1} = \bar{\Omega}_{i+1}\sqrt{1-\xi^2}$. Based on this expression, the phase shift of $\bar{\Omega}^D_{i+1}$ and the numerical damping ratio of $\bar{\xi}_{i+1}$ can be computed by

$$\bar{\Omega}^D_{i+1} = \tan^{-1}\sqrt{\frac{b}{a}}, \quad \bar{\xi}_{i+1} = -\frac{\ln\left(a^2+b^2\right)}{2\bar{\Omega}_{i+1}} \tag{39}$$

where $\bar{\xi}_{i+1}$ is known as a numerical damping ratio. A relative period error is a measure of period distortion and is defined as:

$$P_{i+1} = \frac{\bar{T}_{i+1} - T_{i+1}}{T_{i+1}} = \frac{\omega_{i+1}}{\bar{\omega}_{i+1}} - 1,$$
$$\bar{T}_{i+1} = \frac{2\pi}{\bar{\omega}_{i+1}}, \quad T_{i+1} = \frac{2\pi}{\omega_{i+1}} \tag{40}$$

where T_{i+1} and $\bar{T}_{i+1}$ are the true and computed periods of the system. In general, $\bar{\xi}_{i+1}$ and $\bar{\omega}_{i+1}$ can be considered as the quantities corresponding to ξ_{i+1} and ω_{i+1} in an integration procedure.

Figure 8 shows variations of relative period errors versus $\Delta t/T_0$ for $\sigma = 1$ and 2. In general, the relative period error rises with increasing $\Delta t/T_0$ for given δ and ρ_∞. Period elongation is found for CAM and the amount rises with decreasing ρ_∞ for a given δ while it lessens with the increase of δ for a given ρ_∞. Comparing Fig. 8a, b for each corresponding curve, the relative period error for $\sigma = 2$ is, in general, larger than that of $\sigma = 1$ for a small $\Delta t/T_0$. In fact, it can be shown by numerical experiments that the increase in σ will lead

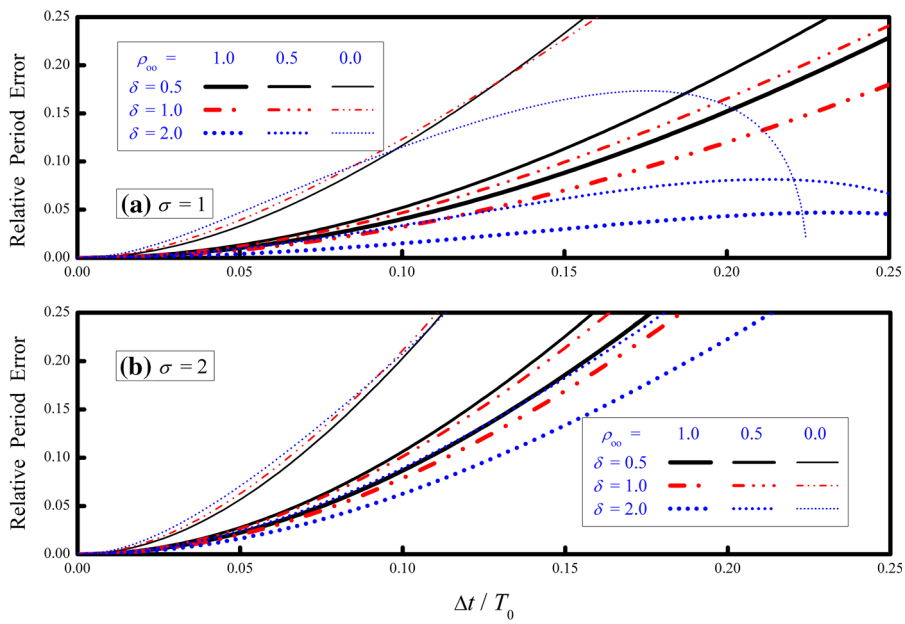

Fig. 8 Variation of relative period error with $\Delta t/T_0$ for different ρ_∞ and δ values

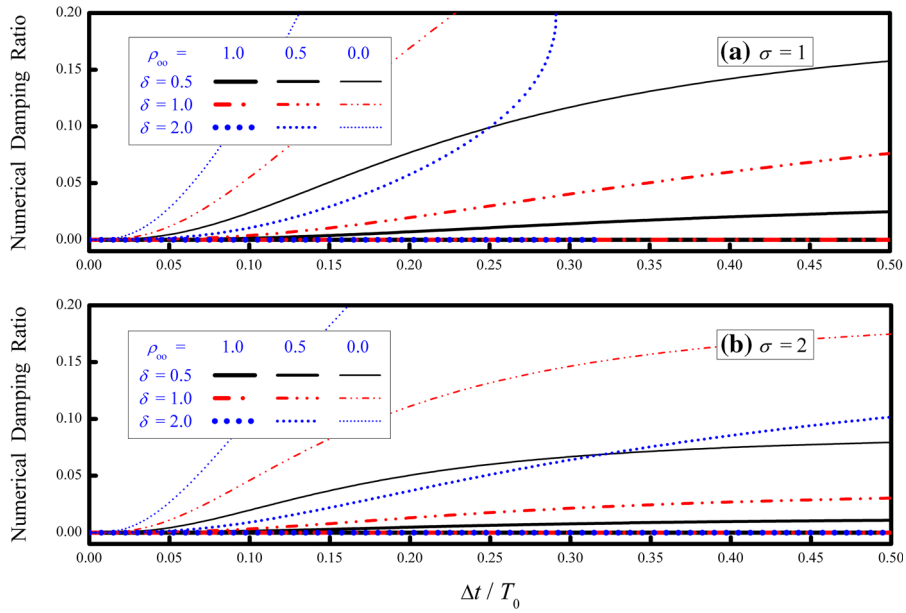

Fig. 9 Variation of numerical damping ratio with $\Delta t/T_0$ for different ρ_∞ and δ values

to the increase of period distortion. Thus, although a large value of σ can extend the unconditional stability interval from $\delta_{i+1} \leq 1$ to $\delta_{i+1} \leq \sigma$, it also results in more period distortion. It is seen in both plots of Fig. 8 that the relative period error is small as $\Delta t/T_0 \leq 0.05$ when ρ_∞ roughly varies in the interval of [0.5, 1]. This implies that CAM with $0.5 \leq \rho_\infty \leq 1$ either for $\sigma = 1$ or 2 can give a reliable solution with an acceptable accuracy for a nonlinear system if $\Delta t/T_0 \leq 0.05$ is met for the modes of interest. As a result, the choice of $\sigma = 2$ is recommended for CAM with $0.5 \leq \rho_\infty \leq 1$ for practical applications. This is because that CAM with $\sigma = 2$ can have an unconditional stability interval of $\delta_{i+1} \leq 2$ and a negligible period distortion as $\Delta t/T_0 \leq 0.05$ if ρ_∞ is chosen to be in the interval of [0.5, 1].

The variation of numerical damping ratio versus $\Delta t/T_0$ for CAM with $\sigma = 1$ and 2 is plotted in Fig. 9. There is zero numerical damping for the case of $\rho_\infty = 1$ for both $\sigma = 1$ and 2, whereas the numerical damping ratio generally rises with $\Delta t/T_0$ and finally tends to a constant for CAM with $\rho_\infty = 0.5$ and 0.0 as $\delta_{i+1} \leq 1$. In addition, it also rises with the decrease in ρ_∞ for a given $\Delta t/T_0$ as $\delta_{i+1} \leq 1$. However, different phenomena are found for the different values of $\sigma = 1$ and 2 for the case of $\delta = 2$. In Fig. 9a, the three curves for $\rho_\infty = 1$, 0.5 and 0.0 will stop at their bifurcation points as $\delta = 2$, where the complex conjugate roots become real roots. On the other hand, in Fig. 9b, the curve for $\rho_\infty = 1$ has zero numerical damping, and the curves for $\rho_\infty = 0.5$ and 0.0 can still have desired numerical damping. In summary, CAM can have a desired numerical damping property if ρ_∞ is chosen from the interval [0, 1] with $\sigma \geq 1$, where the choice of $\sigma = 2$ is generally good enough for practical applications.

Notice that Eqs. (21) and (22) can be applied to define the members of CAM not only for the family of one-step methods but also for the family of two-step methods. Although both equations are derived from the assumption of a triple eigenvalue of $-\rho_\infty$ in the limit $\Omega_0 \to \infty$ as $\sigma = 1$ for a linear elastic system, they are applicable to nonlinear systems and other values of σ since it is revealed by Figs. (7) to (9) that CAM can still have the desired numerical properties for nonlinear systems for the case of $\sigma = 2$.

7 Implementation

Analytical studies reveal that CAM can combine most desirable numerical properties together and thus it seems very competitive with other currently available integration methods. Therefore, it is of great interest to examine its actual performance in solving structural dynamics problems. Some numerical examples are intentionally designed to address the promising numerical properties, such as an unconditional stability,

a second-order accuracy, a good capability of seizing nonlinearity and a good computational efficiency. In addition, the computational efficiency of CAM in contrast to the generalized-α method will be also investigated. For this purpose, a possible implementation of CAM is sketched next for a multiple-degree-of-freedom system. At first, the general formulation of CAM can be simply expressed as:

$$\begin{aligned}
&(1-\alpha_1)\,\mathbf{M}\mathbf{a}_{i+1}+\alpha_1\mathbf{M}\mathbf{a}_i+(1-\alpha_2)\,\mathbf{C}\mathbf{v}_{i+1}\\
&\quad+\alpha_2\mathbf{C}\mathbf{v}_i+(1-\alpha_2)\,\mathbf{K}_{i+1}\mathbf{d}_{i+1}+\alpha_2\mathbf{K}_i\mathbf{d}_i\\
&\quad=(1-\alpha_2)\,\mathbf{f}_{i+1}+\alpha_2\mathbf{f}_i\\
&\mathbf{d}_{i+1}=\mathbf{d}_i-\mathbf{B}_1\,(\Delta t)^2\,\mathbf{K}_i\mathbf{d}_i+\mathbf{B}_2\,(\Delta t)\,\mathbf{v}_i\\
&\quad-\mathbf{B}_1\,(\Delta t)\,\mathbf{C}_i\mathbf{v}_i+\mathbf{B}_3\,(\Delta t)^2\,\mathbf{a}_i+\mathbf{p}_{i+1}\\
&\mathbf{v}_{i+1}=\mathbf{v}_i+(\Delta t)\left[(1-\gamma)\,\mathbf{a}_i+\gamma\mathbf{a}_{i+1}\right]
\end{aligned}\tag{41}$$

where

$$\begin{aligned}
&\mathbf{B}_1=\mathbf{D}^{-1}\beta\\
&\mathbf{B}_2=\mathbf{D}^{-1}\left[(1-\alpha_1)\,\mathbf{M}+(1-\alpha_2)\,\gamma\,(\Delta t)\,\mathbf{C}_0\right]\\
&\mathbf{B}_3=\mathbf{D}^{-1}\left\{\left[\frac{1}{2}(1-\alpha_1)-\beta\right]\mathbf{M}\right.\\
&\qquad\left.-(1-\alpha_2)\left(\beta-\frac{1}{2}\gamma\right)(\Delta t)\,\mathbf{C}_0\right\}\\
&\mathbf{p}_{i+1}=\mathbf{D}^{-1}\,(1-\alpha_2)\,\beta\sigma\,(\Delta t)^2\,(\mathbf{f}_{i+1}-\mathbf{f}_i)\\
&\qquad+\mathbf{D}^{-1}\beta\,(\Delta t)^2\,\mathbf{f}_i
\end{aligned}\tag{42}$$

where $\mathbf{D}=(1-\alpha_1)\,\mathbf{M}+(1-\alpha_2)\left[\gamma\,(\Delta t)\,\mathbf{C}_0+\beta\sigma\,(\Delta t)^2\,\mathbf{K}_0\right]$; $\mathbf{K}$, $\mathbf{C}$ and $\mathbf{M}$ represent the stiffness, viscous damping and mass matrices, respectively; $\mathbf{f}_i$, $\mathbf{a}_i$, $\mathbf{v}_i$ and $\mathbf{d}_i$ are in correspondence to the vectors of the external force, acceleration, velocity and displacement at the end of the ith time step. The symbol $\mathbf{K}_0$ is used to denote the initial stiffness matrix, and the stiffness matrix $\mathbf{K}_i$ in the first and second line of Eq. (41) is generally different from $\mathbf{K}_0$ for a nonlinear system since it may vary with time. Consequently, a restoring force vector $\mathbf{r}_i$ is often introduced to replace the product of $\mathbf{K}_i\mathbf{d}_i$ in the step-by-step solution procedure. Notice that a constant viscous damping matrix is often adopted for structural dynamic analysis and thus $\mathbf{C}=\mathbf{C}_0$ is taken.

After completing the time integration of the ith time step, one can have the data $\mathbf{d}_i$, $\mathbf{v}_i$ and $\mathbf{a}_i$. Hence, the computation of the next step can proceed. At first, the second line of Eq. (41) can be applied to determine the next step displacement vector $\mathbf{d}_{i+1}$, and this solution equation can be alternatively written as:

$$\begin{aligned}
&\mathbf{D}\left(\mathbf{d}_{i+1}-\mathbf{d}_i\right)\\
&\quad=-\beta\,(\Delta t)^2\,\mathbf{r}_i+\{(1-\alpha_1)\,\mathbf{M}\\
&\qquad+\left[(1-\alpha_2)\,\gamma-\beta\right](\Delta t)\,\mathbf{C}_0\}\,(\Delta t)\,\mathbf{v}_i\\
&\qquad+\left\{\left[\frac{1}{2}(1-\alpha_1)-\beta\right]\mathbf{M}\right.\\
&\qquad\left.-(1-\alpha_2)\left(\beta-\frac{1}{2}\gamma\right)(\Delta t)\,\mathbf{C}_0\right\}(\Delta t)^2\,\mathbf{a}_i\\
&\qquad+(1-\alpha_2)\,\beta\sigma\,(\Delta t)^2\left(\mathbf{f}_{i+1}-\mathbf{f}_i\right)+\beta\,(\Delta t)^2\,\mathbf{f}_i
\end{aligned}\tag{43}$$

After obtaining the displacement vector $\mathbf{d}_{i+1}$, the corresponding restoring force vector $\mathbf{r}_{i+1}$ can be further determined from a pre-assumed force–displacement relationship. Notice that Eq. (43) can proceed after finding $\mathbf{a}_0$ based on the initial values of $\mathbf{v}_0$, $\mathbf{d}_0$ and $\mathbf{f}_0$ for the one-step family of methods. However, the second line of Eq. (41) will involve the step data for both the ith and $(i-1)$th time step if using the two-step family of methods. Clearly, it is not self-starting. In fact, it is unable to calculate $\mathbf{a}_1$, $\mathbf{v}_1$ and $\mathbf{d}_1$ by using $\mathbf{a}_0$, $\mathbf{v}_0$ and $\mathbf{d}_0$ only. Alternatively, a one-step method must be used to obtain $\mathbf{a}_1$, $\mathbf{v}_1$ and $\mathbf{d}_1$ first and then the two-step family of methods can be applied, subsequently.

Next, the velocity vector $\mathbf{v}_{i+1}$ can be calculated after substituting the first line into the third line in Eq. (41) and is found to be:

$$\begin{aligned}
&\left[(1-\alpha_1)\,\mathbf{M}+(1-\alpha_2)\,\gamma\,(\Delta t)\,\mathbf{C}_0\right]\mathbf{v}_{i+1}\\
&\quad=\left[(1-\alpha_1)\,\mathbf{M}-\alpha_2\gamma\,(\Delta t)\,\mathbf{C}_0\right]\mathbf{v}_i\\
&\qquad+(1-\alpha_1-\gamma)\,\mathbf{M}\,(\Delta t)\,\mathbf{a}_i\\
&\qquad+\gamma\,(\Delta t)\left[(1-\alpha_2)\,\mathbf{f}_{i+1}+\alpha_2\mathbf{f}_i\right.\\
&\qquad\left.-(1-\alpha_2)\,\mathbf{r}_{i+1}-\alpha_2\mathbf{r}_i\right]
\end{aligned}\tag{44}$$

Finally, the equation of motion, i.e., the first line of Eq. (41), can be directly applied to calculate the acceleration vector $\mathbf{a}_{i+1}$ and is:

$$\begin{aligned}
(1-\alpha_1)\,\mathbf{M}\mathbf{a}_{i+1}&=(1-\alpha_2)\,(\mathbf{f}_{i+1}-\mathbf{C}_0\mathbf{v}_{i+1}-\mathbf{r}_{i+1})\\
&\quad+\alpha_2\,(\mathbf{f}_i-\mathbf{C}_0\mathbf{v}_i-\mathbf{r}_i)-\alpha_1\mathbf{M}\mathbf{a}_i
\end{aligned}\tag{45}$$

In general, Eqs. (43) to (45) are solved by a direct elimination method, which has two parts. First, "triangulation" and then "substitution". The triangulation of $\mathbf{D}$, $(1-\alpha_1)\,\mathbf{M}+(1-\alpha_2)\,\gamma\,(\Delta t)\,\mathbf{C}_0$ or $(1-\alpha_1)\,\mathbf{M}$ can be conducted only once at the beginning of time integration. This is because these matrices will remain invariant for a whole integration procedure and thus the factored results can be restored for the subsequent use. It is manifested from an operation count that a triangulation will involve much more operations than for a

substitution in conducting a direct elimination. Hence, the need of only one triangulation of these matrices is the key issue for structure-dependent integration methods to compute efficiently in the nonlinear dynamic analysis. Notice that there is no need to triangulate the matrix **M** in solving Eq. (45) if it is a diagonal matrix. Similarly, the solution of Eq. (44) will involve no triangulation if **M** is a diagonal matrix in addition to $\mathbf{C}_0 = \mathbf{0}$.

8 Numerical examples

To confirm the feasibility of CAM for general nonlinear dynamic analysis, CAM1 and CAM2 will be applied to solve some structural dynamics problems. These numerical results can also attest to some numerical properties of CAM. In general, the results calculated from CAM will compare with the results obtained from a conventional, second-order accurate integration method to illustrate that CAM generally has a comparable accuracy.

8.1 A mathematically nonlinear system

There is a mathematically nonlinear system, whose instantaneous degree of nonlinearity highly depends upon the specified initial conditions. This system is very useful for assessing the capability of an integration method for seizing the rapid variation of nonlinearity. The governing equation of motion for the nonlinear system can be simply expressed as:

$$\ddot{u} + \frac{u}{1+|u|} = A \sin(\bar{\omega} t) \tag{46}$$

The stiffness has an initial natural frequency $\omega = 1$ rad/s and will be softening after the system deforms. In addition, a large initial displacement or velocity will result in a large reduction in the stiffness. The system has an initial structural period of 2π s. Free vibration responses to the initial conditions of $u(0) = 0$, $\dot{u}(0) = 100$ and $A = 0$ are displayed in Fig. 10a and the time history of δ_{i+1} is plotted in Fig. 10b. Besides, the frequency response curves for $A = 0.3$ with $0 < \bar{\omega} \leq 0.5$ are also calculated and the results

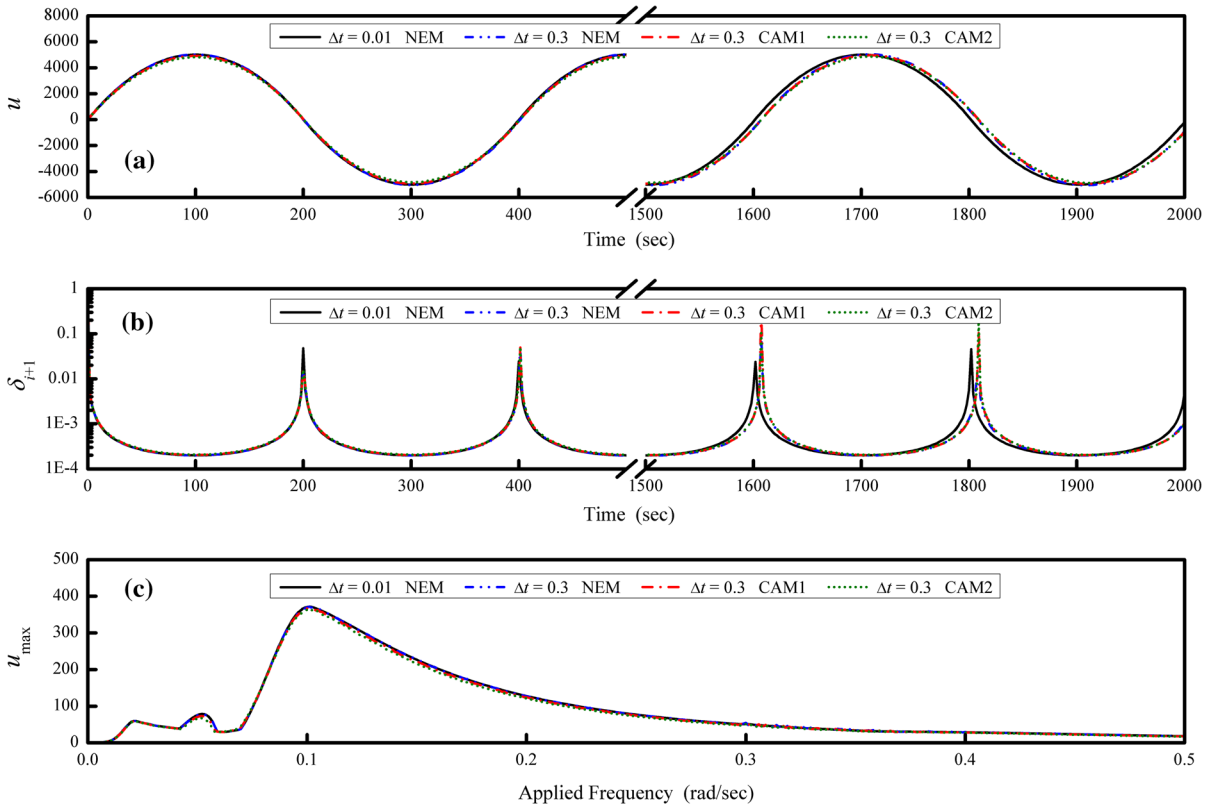

Fig. 10 Responses to mathematically nonlinear system

are plotted in Fig. 10c. The result obtained from NEM with $\Delta t = 0.01$ s is treated as a reference solution. Both CAM1 and CAM2 are applied to conduct time integration. It is seen in Fig. 10a that the solutions obtained from CAM1 and CAM2 are reliable and have a comparable accuracy with that obtained from NEM. Figure 10b reveals that the system has been experienced a high stiffness softening since δ_{i+1} varies in the interval of $[10^{-4}, 1]$. Notice that not all the structure-dependent integration methods can have such a good capability of seizing the rapid variation of the structural nonlinearity. In fact, some of them do not possess such a good capability as shown in the reference [38,44–47], such as the CR explicit method [31] and KR-α method [37]. It is manifested from Fig. 10c that CAM1 and CAM2 can also give comparable solutions in contrast to NEM in calculating the frequency response curves, where a peak response is close to $\bar{\omega} = 0.1$. It is indicated that the system experiences significantly stiffness softening since the resonant response occurred around $\bar{\omega} = 0.1$, which implies that the natural frequency of the system varies from $\omega = 1$ rad/s to roughly about $\omega = 0.1$ rad/s due to stiffness softening.

8.2 An elastoplastic system

A one-story shear-beam-type building is excited by the earthquake record of TCU084, which was recorded during the main shock of Chi–Chi earthquake in Taiwan. This building is simulated by a single-degree-of-freedom system and its lumped mass and stiffness are assumed to be 10^5 kg and 10^6 N/m, respectively. As a result, the natural frequency of the system is found to be 3.16 rad/s before it deforms. An elastoplastic behavior is assumed for the building during vibration and the yielding strength is taken as 3×10^4 N for both tension and compression. Zero viscous damping is considered for the building and the peak ground acceleration of the seismic input of TCU084 was scaled to 0.5 g.

Figure 11 shows the calculated seismic responses. The results obtained from NEM with a time step of $\Delta t = 0.005$ s are considered as reference solutions.

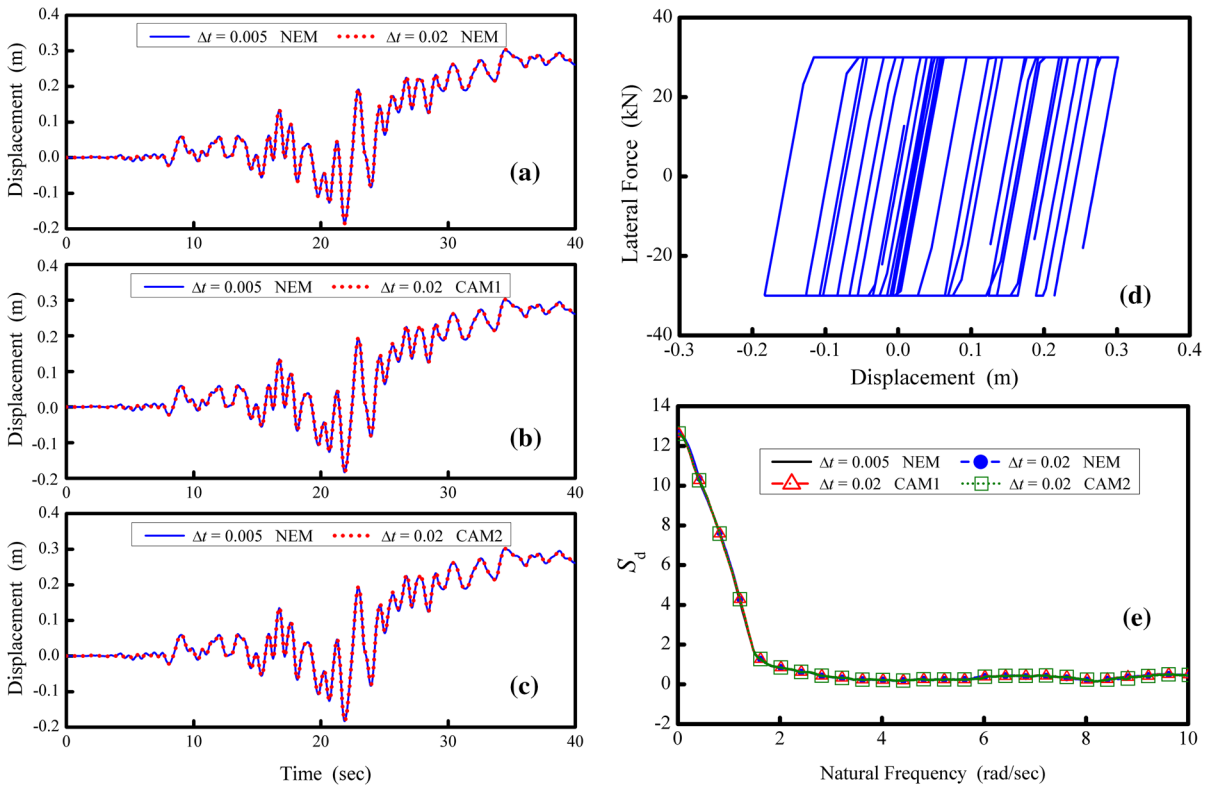

Fig. 11 Responses to TCU084 for one-story shear-beam-type building

Meanwhile, NEM, CAM1, and CAM2 with a time step of $\Delta t = 0.02\,\mathrm{s}$ are also applied to compute the responses. It is seen in Fig. 11a, c that the results obtained from NEM, CAM1, and CAM2 overlap the reference solutions. Thus, either CAM1 or CAM2 can capture the rapid changes of the stiffness and ground shaking caused by an earthquake, and then it gives the results that have a comparable accuracy with NEM. An elastoplastic behavior of the building is found in Fig. 11d, where the hysteresis loops are very complicated. The variation of spectral displacement S_d with natural frequency ω is also plotted in Fig. 11e. It is evident that both CAM1 and CAM2 can provide reliable seismic responses for different natural frequencies of the systems as each system experiences an elastoplastic behavior.

8.3 A 7-story building

To illustrate that CAM can have desired numerical damping to suppress or even eliminate the high-frequency responses, a 7-story shear-beam-type building is intentionally designated to have a relatively high-frequency mode. The stiffness of each story generally consists of a linear part and a nonlinear part. A constant stiffness is taken for the linear part and the nonlinear part is assumed to be a function of the story drift. The explicit expression of the stiffness for each story can be written in the form of:

$$k = k_0 \left(1 + q\sqrt{|\Delta u|}\right) \tag{47}$$

where k_0 is the initial stiffness; q is an arbitrary constant and Δu is a story drift. Clearly, the choice of a positive value of q will result in stiffness hardening. The structural properties of the building are shown in Fig. 12. As a result, the lowest and the highest initial natural frequencies of the building are 13.96 and 3178.21 rad/s, and their corresponding mode shapes are found to be $\phi_1 = [0.44,\ 0.80,\ 0.99,\ 0.99,\ 1.00,\ 1.00,\ 1.00]^{\mathrm{T}}$ and $\phi_7 = [0.00,\ 0.00,\ 0.00,\ 0.00,\ 0.00,\ -0.01,\ 1.00]^{\mathrm{T}}$.

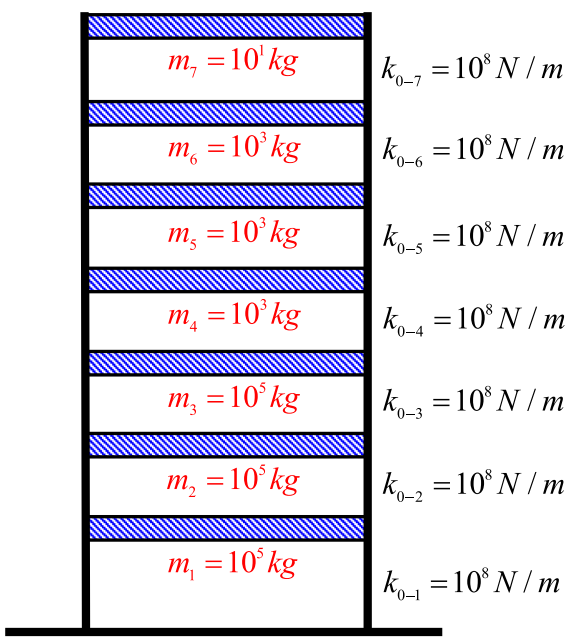

Fig. 12 A 7-story building and its vibration properties

The free vibration responses of two different combinations of initial conditions are calculated from using CAM1 and CAM2. This is intended to illustrate that both integration methods can have a desired numerical damping to repress high-frequency responses, while low-frequency responses can still be very accurately integrated. For this purpose, two combinations of initial conditions of C-1 and C-2 are considered:

$$\begin{aligned} &\text{C-1}: \quad \mathbf{u}(0) = \phi_1/10 \quad \text{and} \quad \dot{\mathbf{u}}(0) = 0 \\ &\text{C-2}: \quad \mathbf{u}(0) = (\phi_1+\phi_7)/10 \quad \text{and} \quad \dot{\mathbf{u}}(0) = 0 \end{aligned} \tag{48}$$

where ϕ_1 and ϕ_7 are the 1st and 7th modal shapes of the building as shown in Fig. 12. Clearly, C-1 has the pure first mode only, while C-2 consists of the first mode and seventh mode with equal weight. The component from the 7th mode can be considered as a high-frequency disturbance. In this study, $q = 1.5$ is chosen for each story to mimic a stiffness hardening system. The free vibration response of C-1 obtained from AAM with $\Delta t = 0.001\,\mathrm{s}$ is treated as a reference solution since it involves no response contribution from the 7th mode and can be very accurately integrated. This time step can meet the upper stability limit $\omega_0^{(7)}(\Delta t) = 1.59 < 2$ and thus a stable result can be achieved. In addition, it is also small enough to accurately integrate the 1st mode and thus gives reliable solutions. On the other hand, the free vibration responses of C-2 are computed by using AAM, CAM1 and CAM2 with a time step of $\Delta t = 0.01\,\mathrm{s}$. Notice that CAM1 and CAM2 can have desired numerical damping while AAM is non-dissipative.

It is recognized that a nonlinear multiple-degree-of-freedom system cannot be decomposed into uncoupled single-degree-of-freedom systems for a complete integration procedure. However, it can be done for

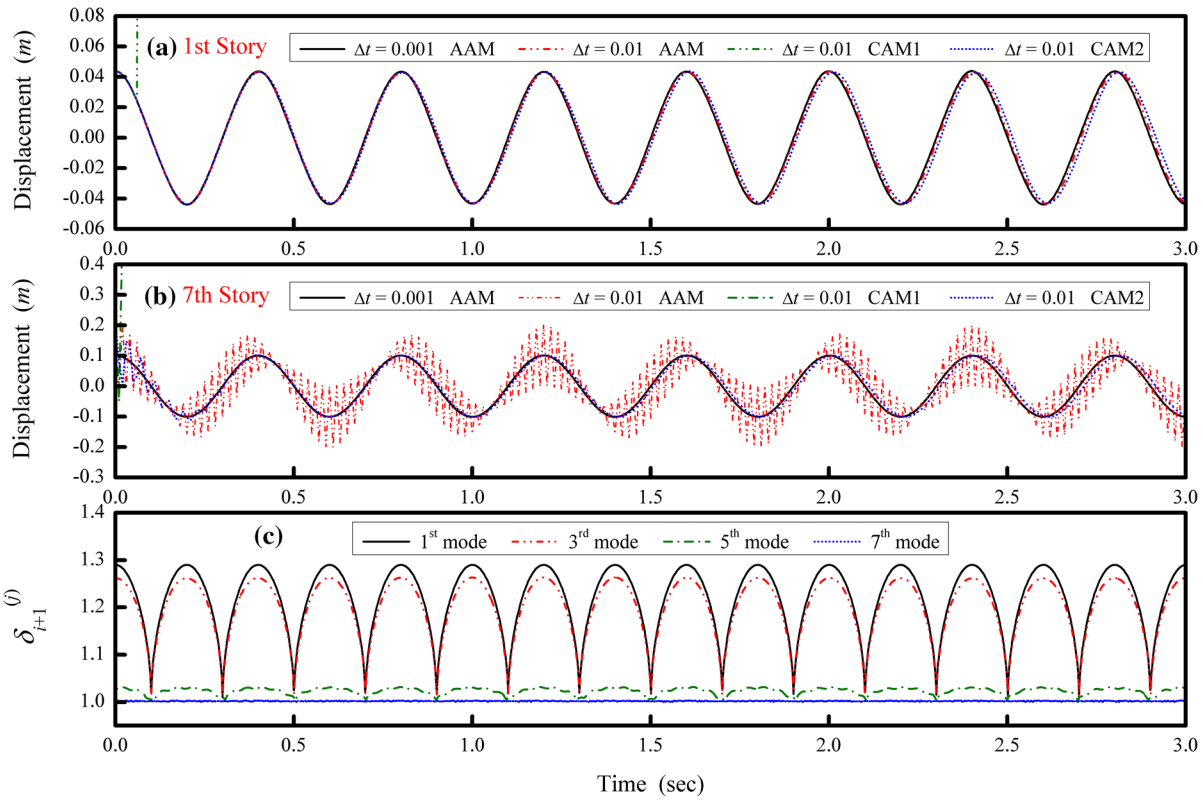

Fig. 13 Free vibration responses of 7-story building

each time step. Hence, the numerical properties of an integration method for solving a nonlinear single-degree-of-freedom system are applicable to the uncoupled single-degree-of-freedom systems. This application requires the natural frequencies of the modes of interest for each time step and the corresponding instantaneous degree of nonlinearity of these modes. The natural frequencies of each time step can be used to determine the instantaneous degrees of nonlinearity for the modes of interest correspondingly. In fact, the following formula can be used to compute the instantaneous degree of nonlinearity at the $(i+1)$th time step for the jth mode:

$$\delta_{i+1}^{(j)} = \left[\frac{\omega_{i+1}^{(j)}}{\omega_0^{(j)}}\right]^2 \tag{49}$$

where $\omega_0^{(j)}$ is the natural frequency of the jth mode based on the initial stiffness and $\omega_{i+1}^{(j)}$ is that based on the stiffness at the end of the $(i+1)$th time step. The extreme value of $\delta_{i+1}^{(j)}$ plays a key role for determining the upper stability limit for CAM as shown in Fig. 2 and the numerical properties of CAM for nonlinear systems can be found from Figs. 7 to 9. Hence, these properties can be applied to thoroughly explain the numerical solutions of this problem.

The free vibration responses obtained from CAM1 and CAM2 are shown in Fig. 13a, b, respectively. In addition, the time variation of instantaneous degree of nonlinearity for each mode is also calculated by using Eq. (49) and is plotted in Fig. 13c. In Fig. 13a, AAM and CAM2 can give reliable solutions for the first story while an instability occurs for the results obtained from CAM1. Different phenomena are found in Fig. 13b, where AAM no longer gives reliable results although CAM1 also leads to an instability and CAM2 can still give acceptable results. Figure 13c reveals that each mode experiences stiffness hardening. Thus, an instability occurred in the results obtained from CAM1 is caused by the violation of the upper stability limit since CAM1 only has a conditional stability for stiffness hardening systems, i.e., for $\delta_{i+1}^{(j)} > 1$. In contrast, CAM2 can have an unconditional stability in the inter-

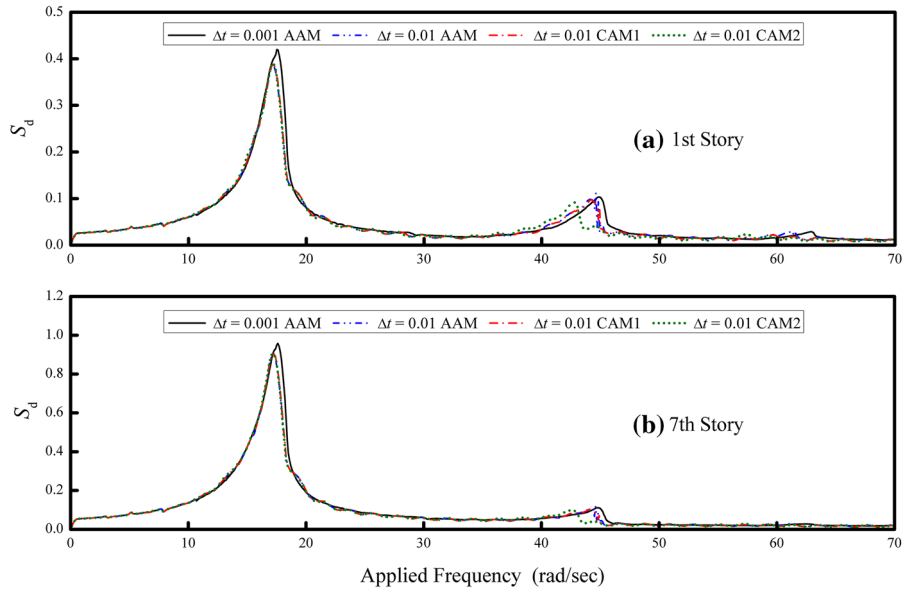

Fig. 14 Frequency response curves for 7-story building

val of $0 < \delta_{i+1}^{(j)} \leq 2$ and thereby there is no instability since $0 < \delta_{i+1}^{(j)} \leq 1.3$ is found. Notice that AAM can provide accurate results for the first story while a very significant error is found for the seventh story response. This is mainly because that the seventh mode only significantly contribute to the 7th story while it contributes insignificantly to the other stories. This can be manifested from the 7th mode shape ϕ_7. Clearly, the first story response is unaffected by the initial disturbance of $\phi_7/10$, while the seventh story response is contaminated by it since AAM has no numerical damping to filter out the high-frequency disturbance. It is manifested from Fig. 13b that CAM2 has a desired numerical damping to take out the high-frequency disturbance.

In addition to the free vibration analysis, the forced vibration analysis of the building is also conducted, where the building is excited by a ground acceleration of $10\sin(\bar{\omega}t)$ at its base. As a result, the variation of the spectral displacement at the bottom and top stories versus the applied frequency $\bar{\omega}$ is plotted in Fig. 14. The frequency response curve obtained from AAM with the time step of $\Delta t = 0.001\,\text{s}$ is considered as a reference solution. Whereas, $\Delta t = 0.01\,\text{s}$ is adopted for AAM, CAM1, and CAM2. Clearly, both CAM1 and CAM2 also have comparable solutions when compared to AAM. Notice that the first peak response occurs at $\bar{\omega} = 17.5\,\text{rad/s}$ but not the initial first mode $\omega_1 = 13.96\,\text{rad/s}$ is due to the stiffness hardening.

8.4 An elastic pendulum

An elastic pendulum is considered, where $l = \sqrt{(u_1)^2 + (u_2)^2}$ denotes the instantaneous length of the pendulum and l_0 is the length of the unstretched pendulum. In general, the equation of motion [48] can be generally expressed as:

$$\begin{bmatrix} m & 0 \\ 0 & m \end{bmatrix} \begin{Bmatrix} \Delta\ddot{u}_1 \\ \Delta\ddot{u}_2 \end{Bmatrix} + \begin{bmatrix} k\left[1 - \frac{l_0}{l} + \frac{l_0 (u_1)^2}{l^3}\right] & k\frac{l_0 u_1 u_2}{l^3} \\ k\frac{l_0 u_1 u_2}{l^3} & k\left[1 - \frac{l_0}{l} + \frac{l_0 (u_2)^2}{l^3}\right] \end{bmatrix} \times \begin{Bmatrix} \Delta u_1 \\ \Delta u_2 \end{Bmatrix} = \begin{Bmatrix} 0 \\ 0 \end{Bmatrix} \tag{50}$$

where $m = 1\,\text{kg}$, $k = 30\,\text{N/m}$, $l_0 = 1\,\text{m}$ and $g = 10\,\text{m/s}^2$ are assumed. Clearly, these equations of motion are highly nonlinear since the pendulum length is deformable in its axial direction. The initial values are taken to be $u_1(0) = 1.5\,\text{m}$, $u_2(0) = 0$, $\dot{u}_1(0) = 0$ and $\dot{u}_2(0) = 0$. The numerical solution obtained from AAM with $\Delta t = 0.001\,\text{s}$ is considered as a reference solution. In addition, AAM, CAM1, and CAM2 with $\Delta t = 0.01\,\text{s}$ is also applied to compute the responses and the results are plotted in Fig. 15. It is seen in Fig. 15a, b that CAM1 and CAM2 result in comparable solutions as those obtained from AAM. Figure 15c shows the trajectory of the pendulum, where u_1 varies within $\pm 1.65\,\text{m}$ while u_2 is bounded in the interval of

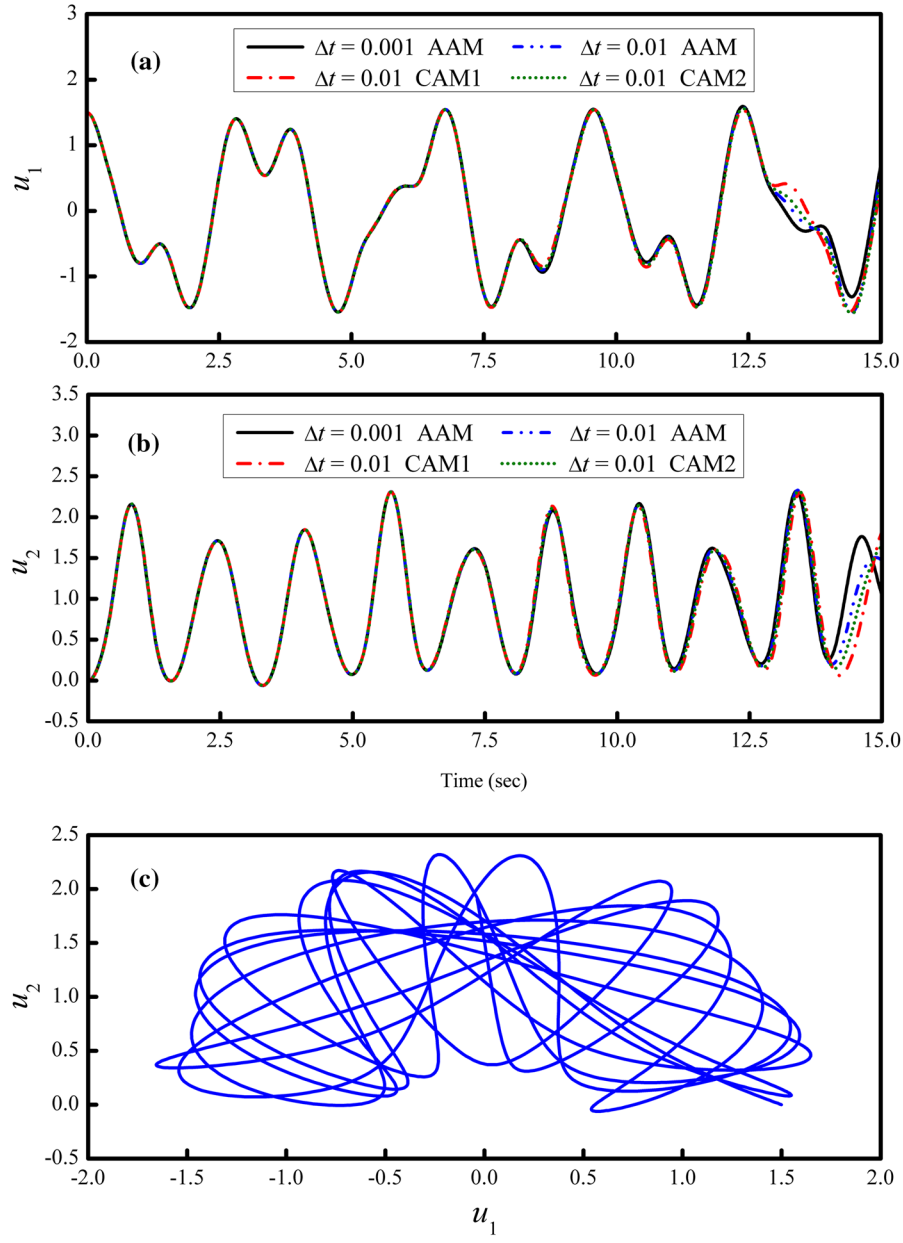

Fig. 15 Responses of elastic pendulum

$0 \leq u_2 \leq 2.35\,\text{m}$. Thus, it is evident that CAM can be generally applied to solve highly nonlinear systems.

8.5 Computational efficiency

A very important characteristic of a general structure-dependent integration method is that it not only has unconditional stability but also explicit formulation. An unconditional stability allows selecting a time step without considering stability problem, and an explicit formulation will involve no nonlinear iterations. Hence, many computational efforts are expected to be saved for solving an inertial problem. A spring–mass system with arbitrarily specific degrees of freedom can be applied to substantiate this prediction. The system is schematically shown in Fig. 16, where $m_i = 10^2\,\text{kg}$ and $k_i = 10^8\left(1 - \sqrt{|u_i - u_{i-1}|}\right)\text{N/m}$. In general, the spring stiffness k_i will decrease after the system deforms due to the nonlinear term $-10^8\sqrt{|u_i - u_{i-1}|}$.

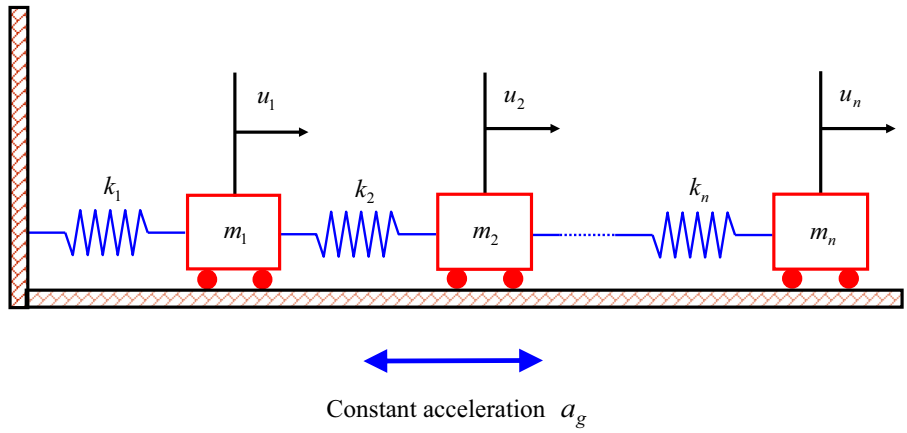

Fig. 16 A n-degree-of-freedom spring–mass system

Table 1 The lowest and highest natural frequencies and time integration data

n	$\omega_0^{(1)}$(rad/s)	$\omega_0^{(n)}$ (rad/s)	a_g (m/s^2)	Δt (s)	t_d (s)	N
200	7.83	2000.00	16.0	0.02	4	200
400	3.92	2000.00	4.0	0.04	8	200
800	1.96	2000.00	1.0	0.08	16	200
1600	0.98	2000.00	0.25	0.16	32	200

As a result, the case of $\delta_{i+1}^{(j)} < 1$ is generally found for each mode at each time step.

Four different n values of 200, 400, 800, and 1600 are specified for the spring-mass system so that four different systems with the degrees of freedom of 200, 400, 800, and 1600 can be simulated. A constant acceleration a_g will be inputted into each system at its base. This simple external force is intended to avoid the difficulty in faithfully seizing the applied dynamic loading. The lowest and highest initial natural frequencies and constant acceleration for each system are listed in Table 1. This is a typical inertial problem and the highest natural frequency of each system is as large as 2000.0 rad/s. A dissipative, explicit, unconditionally stable integration method is promising for solving such an inertial problem. As a result, the generalized$-\alpha$ method with $\rho_\infty = 1/2$ (GAM) and CAM2 are selected for the numerical calculations. In addition, NEM with $\Delta t = 0.001$ s is also adopted to calculate the response for each system. The criterion for choosing this time step is to satisfy the upper stability limit, i.e., $\omega_0^{(n)}(\Delta t) = 2000 \times 0.001 = 2 \leq 2$. Clearly, this time step is much smaller than that required by accuracy consideration and thus the result obtained from NEM can be considered as a reference solution for each system. In contrast to NEM, there is no limitation on the step size for GAM and CAM2 since they are unconditionally stable. Hence, a time step can be selected based on accuracy consideration. In these numerical experiments, the total number of time steps of $N = 200$ is taken for each system. Hence, the loading duration of each system is found to be $t_d = 200 \times (\Delta t)$. For each system, the step size Δt, loading duration t_d and the conducted total number of time steps N are also listed in Table 1.

The responses of the four systems are shown in Fig. 17. Comparing the results obtained from GAM and CAM2 to the reference solutions for each plot of this figure, it seems that $\Delta t = 0.02$, 0.04, 0.08 and 0.16 s are the maximum allowable time steps to yield reliable results corresponding to the 200-DOF, 400-DOF, 800-DOF, and 1600-DOF systems. The result obtained from CAM2 is in good agreements with those obtained from GAM for each system using the same step size. This attests that CAM2 can have a comparable accuracy with GAM. In addition, the unconditional stability of CAM2 is also indicated in this example since the value of $\omega_0^{(n)}(\Delta t)$ for the highest mode of each system is as large as 40, 80, 160, and 320 corresponding to the 200-DOF, 400-DOF, 800-DOF, and 1600-DOF systems.

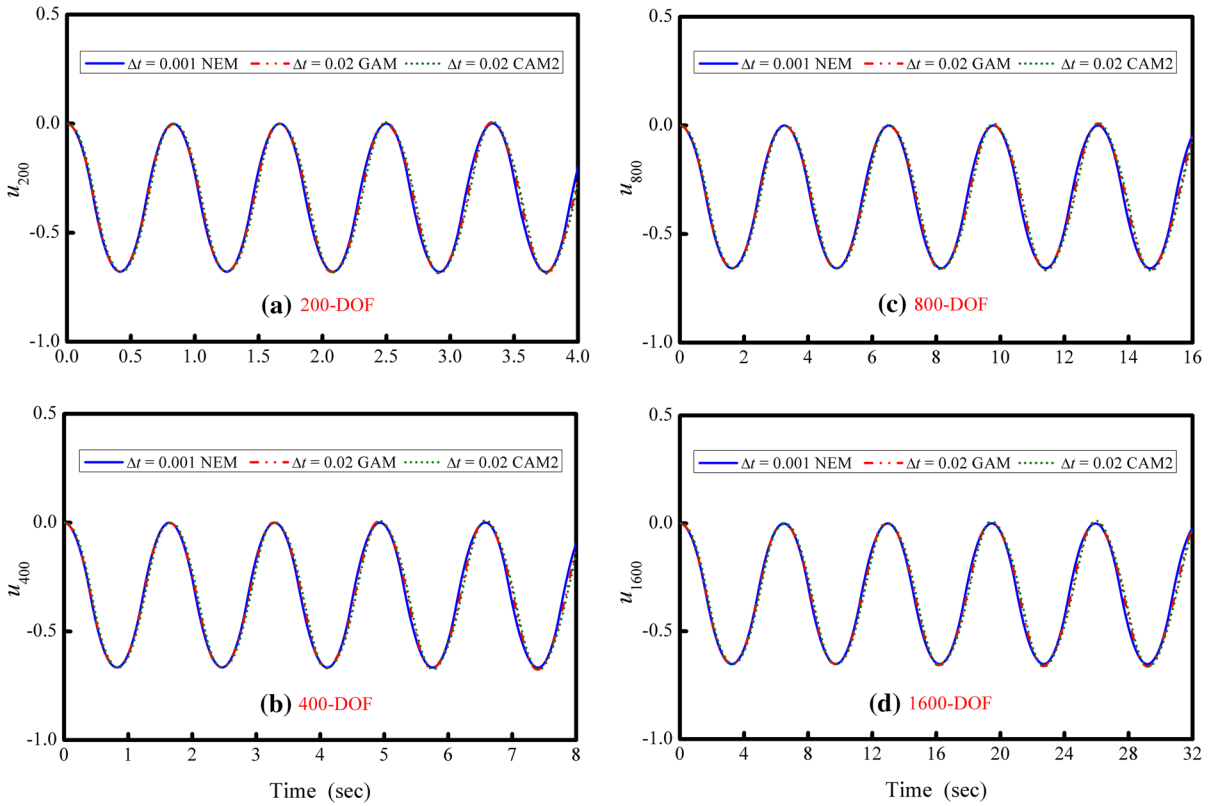

Fig. 17 Displacement responses of four systems subject to constant acceleration

For each dynamic analysis, the consumed CPU time is recorded and listed in Table 2 for GAM and CAM2 so that the computational efficiency of CAM2 can be evaluated and compared with that of GAM. The third column reveals that CAM2 consumes much less CPU time when compared with GAM. The difference between CAM2 and GAM is that CAM2 involves no nonlinear iterations for each time step while an iteration procedure is needed for GAM and it costs a lot of CPU time for a matrix of large order as shown in the 2nd columns. This attests that CAM2 is very computationally efficient in contrast to GAM. A consumed CPU time ratio is defined as the CPU time involved by CAM2 over that consumed by GAM. The last column shows that the ratio lessens with increasing number of the degrees of freedom. Thus, the computational efficiency of CAM2 increases as the total number of the degrees of freedom of the system increases. In general, the ratio as shown in the last column is 1% for the 200-DOF system, while it is as small as 0.26% for the 1600-DOF system.

Table 2 Comparison of CPU time

N-DOF	GAM	CAM2	$\frac{\text{CAM2}}{\text{GAM}}$
200	22.86	0.23	0.0100
400	176.17	1.17	0.0066
800	1917.34	7.67	0.0040
1600	17, 732.14	45.33	0.0026

The computations that involve main computational efforts at each time step of GAM and CAM are examined so that the drastic difference in CPU time between these two methods can be revealed. The Newton–Raphson method is often applied to iteratively compute the current step displacement vector for an implicit method, such as the generalized-α method adopted in this work. In general, a direct elimination method is applied to solve a system of linear equations for each iteration, where a triangulation, a substitution and a stiffness matrix update might be involved. As a result, the total number of the triangulation, substitution and

Table 3 Comparison of major consumed computational efforts between generalized-α method and CAM

N-DOF	GAM						CAM			
	Total number of time steps	Average number of iterations	Total number of iterations	Total number of triangulations	Total number of substitutions	Total number of stiffness updates	Total number of time steps	Total number of triangulations	Total number of substitutions	Total number of stiffness updates
200	200	3.235	647	647	647	647	200	1	200	200
400	200	2.995	599	599	599	599	200	1	200	200
800	200	2.995	599	599	599	599	200	1	200	200
1600	200	2.995	599	599	599	599	200	1	200	200

stiffness matrix updates are equal to the total number of the nonlinear iterations per time step. In contrast, for a structure-dependent integration method, such as CAM, the triangulation is conducted only once at the start of time integration. Thus, only a substitution and a stiffness matrix update are generally needed for each time step. Notice that for a large system a triangulation will consume much more CPU time than that of a substitution. In fact, the cost of a substitution might be negligible in contrast to a triangulation for a large system.

The total number of the triangulation, substitution and stiffness matrix update are summarized in Table 3 for comparison for both GAM and CAM. It is seen in columns 5 and 9 that the total number of triangulation for GAM is about 600 for each system, where a convergent solution can be obtained after about three iterations for each time step, while it is only 1 for CAM. In addition, the total number of substitution and stiffness update for GAM is also about 600 for each system while it is 200 for CAM. Clearly, the difference in the total number of the triangulation is the root cause to the drastic difference in CPU time. In addition, the total number of the substitution or stiffness update for CAM is only about one-third of that required by GAM. Consequently, CAM is very computationally efficient in contrast to GAM.

9 Subfamily of CAM

A free parameter ρ_∞ can be applied to control the numerical properties of CAM and it can be considered as an index of the amount of the high-frequency numerical damping. Clearly, $\rho_\infty = 1$ implies no numerical damping. Hence, ρ_∞ close to 1 implies a small numerical damping while a large numerical damping is indicated as ρ_∞ close to 0. In addition, CAM can degenerate into two subfamilies of one-step, dissipative methods and a subfamily of non-dissipative methods.

In general, the First Subfamily Method (FSM) can be reduced from CAM by simply taking $\alpha_1 = 0$ and $\alpha_2 = -\alpha$. As a result, Eq. (11) becomes:

$$\begin{aligned} & ma_{i+1} + (1+\alpha)\, cv_{i+1} - \alpha cv_i + (1+\alpha)\, kd_{i+1} \\ & \quad - \alpha kd_i = (1+\alpha)\, f_{i+1} - \alpha f_i \\ & d_{i+1} = d_i - \bar{\beta}_1 \Omega_i^2 d_i + \bar{\beta}_2\, (\Delta t)\, v_i \\ & \quad - \bar{\beta}_1 2\xi \Omega_i\, (\Delta t)\, v_i + \bar{\beta}_3\, (\Delta t)^2\, a_i + \bar{p}_{i+1} \\ & v_{i+1} = v_i + (\Delta t) \left[(1-\gamma)\, a_i + \gamma a_{i+1} \right] \end{aligned} \tag{51}$$

where the coefficients of $\bar{\beta}_1$ to $\bar{\beta}_3$ and $\bar{p}_{i+1}$ can be reduced from Eq. (12) and are:

$$\begin{aligned}
\bar{\beta}_1 &= \frac{1}{D}\beta \\
\bar{\beta}_2 &= \frac{1}{D}\left[1+(1+\alpha)\,\gamma 2\xi\Omega_0\right] \\
\bar{\beta}_3 &= \frac{1}{D}\left[\left(\frac{1}{2}-\beta\right)-(1+\alpha)\left(\beta-\frac{1}{2}\gamma\right)2\xi\Omega_0\right] \\
\bar{p}_{i+1} &= \frac{1}{D}(1+\alpha)\,\beta\sigma\frac{1}{m}(\Delta t)^2(f_{i+1}-f_i)\,f_{i+1} \\
&\quad +\frac{1}{D}\beta\frac{1}{m}(\Delta t)^2 f_i
\end{aligned} \tag{52}$$

where $D = 1+(1+\alpha)\left(2\gamma\xi\Omega_0+\beta\sigma\Omega_0^2\right)$. In addition, the following relationships can be determined from the same procedure described in the subsection of stability:

$$-\frac{1}{3}\le\alpha\le 0,\quad \beta=\frac{1}{4}(1-\alpha)^2,\quad \gamma=\frac{1}{2}-\alpha \tag{53}$$

The member of this subfamily generally has desired numerical damping except for $\alpha = 0$. Notice that $\alpha = 0$, which leads to $\beta = 1/4$ and $\gamma = 1/2$, generally denotes a non-dissipative integration method. Both CAM1 and CAM2 can be also treated as the members of this subfamily of methods by taking $\alpha = -1/3$ with $\sigma = 1$ and $\sigma = 2$. Meanwhile, the second subfamily method (SSM) can be also obtained from CAM by taking $\alpha_1 = \alpha$ and $\alpha_2 = 0$. As a result, Eq. (11) becomes:

$$\begin{aligned}
&(1-\alpha)\,ma_{i+1}+\alpha ma_i+cv_{i+1}+kd_{i+1}=f_{i+1} \\
&d_{i+1}=d_i-\bar{\beta}_1\Omega_i^2 d_i+\bar{\beta}_2(\Delta t)\,v_i \\
&\quad -\bar{\beta}_1 2\xi\Omega_i(\Delta t)\,v_i+\bar{\beta}_3(\Delta t)^2 a_i+\bar{p}_{i+1} \\
&v_{i+1}=v_i+(\Delta t)\left[(1-\gamma)\,a_i+\gamma a_{i+1}\right]
\end{aligned} \tag{54}$$

where

$$\begin{aligned}
\bar{\beta}_1 &= \frac{1}{D}\beta \\
\bar{\beta}_2 &= \frac{1}{D}\left[(1-\alpha)+2\gamma\xi\Omega_0\right] \\
\bar{\beta}_3 &= \frac{1}{D}\left\{\left[\frac{1}{2}(1-\alpha)-\beta\right]-\left(\beta-\frac{1}{2}\gamma\right)2\xi\Omega_0\right\} \\
\bar{p}_{i+1} &= \frac{\beta}{D}\sigma\frac{1}{m}(\Delta t)^2(f_{i+1}-f_i)+\frac{\beta}{D}\frac{1}{m}(\Delta t)^2 f_i
\end{aligned} \tag{55}$$

where $D = (1-\alpha)+2\gamma\xi\Omega_0+\beta\sigma\Omega_0^2$. Similarly, the following relationships can be also determined from the same procedure:

$$-1\le\alpha\le 0,\quad \beta=\frac{1}{4}(1-\alpha)^2,\quad \gamma=\frac{1}{2}-\alpha \tag{56}$$

Clearly, a non-dissipative integration method can be obtained by taking $\alpha = 0$, which also results in $\beta = 1/4$ and $\gamma = 1/2$, while the choice of $\alpha \neq 0$ generally represents a dissipative integration method. Notice that these two subfamilies no longer have a triple root of the characteristic equation in the limit $\Omega_0 \to \infty$ but a pair of principal roots in addition to a spurious root.

In general, the spectral radius ρ_∞ in the limit $\Omega_0 \to \infty$ can be considered as an indicator for the amount of high-frequency numerical damping, it is of great interest to construct the correlations between α and ρ_∞ for both FSM and SSM. As a result, they are found to be:

$$\begin{aligned}
&\alpha=\frac{\rho_\infty-1}{\rho_\infty+1},\quad \frac{1}{2}\le\rho_\infty\le 1 \quad \text{FSM} \\
&\alpha=\frac{\rho_\infty-1}{\rho_\infty+1},\quad 0\le\rho_\infty\le 1 \quad \text{SSM}
\end{aligned} \tag{57}$$

The variation of α from $-1/3$ to 0 is in correspondence to the variation of ρ_∞ from 1/2 to 1 for FSM. Similarly, the variation of α from -1 to 0 is correspondent to the variation of ρ_∞ from 0 to 1 for SSM. It is evident that both FSM and SSM can have a controllable numerical dissipation. Notice that a zero-damping ratio can be generally obtained for both dissipative families of methods.

Finally, a non-dissipative family of methods can be further obtained from either FSM or SSM by taking $\alpha = 0$ and $\sigma = 1$. In addition, it can also be derived from CAM by taking $\alpha_1 = \alpha_2 = 0$ and $\sigma = 1$. As a result, it is found to be:

$$\begin{aligned}
&ma_{i+1}+cv_{i+1}+kd_{i+1}=f_{i+1} \\
&d_{i+1}=d_i-\bar{\beta}_1\Omega_i^2 d_i+\bar{\beta}_2(\Delta t)\,v_i \\
&\quad -\bar{\beta}_1 2\xi\Omega_i(\Delta t)\,v_i+\bar{\beta}_3(\Delta t)^2 a_i+\bar{p}_{i+1} \\
&v_{i+1}=v_i+(\Delta t)\left[(1-\gamma)\,a_i+\gamma a_{i+1}\right]
\end{aligned} \tag{58}$$

Clearly, an asymptotic equation of motion is no longer involved. Alternatively, an exact equation of motion is involved for this non-dissipative family of methods. In addition, the coefficients of $\bar{\beta}_1$ to $\bar{\beta}_3$ and $\bar{p}_{i+1}$ become:

$$\begin{aligned}
\bar{\beta}_1 &= \frac{1}{D}\beta \\
\bar{\beta}_2 &= \frac{1}{D}(1+\gamma 2\xi\Omega_0) \\
\bar{\beta}_3 &= \frac{1}{D}\left[\left(\frac{1}{2}-\beta\right)-\left(\beta-\frac{1}{2}\gamma\right)2\xi\Omega_0\right] \\
\bar{p}_{i+1} &= \frac{1}{D}\beta\frac{1}{m}(\Delta t)^2 f_{i+1}
\end{aligned} \tag{59}$$

where $D = 1 + 2\gamma\xi\Omega_0 + \beta\Omega_0^2$. In general, the parameters β and γ can be appropriately selected and are no longer constrained by either Eqs. (53) or (56). After substituting Eq. (59) into the second line of Eq. (58), it will become:

$$\begin{aligned} d_{i+1} &= d_i + \frac{1}{D}\left(1 + 2\gamma\xi\Omega_0\right)(\Delta t)\, v_i \\ &\quad + \frac{1}{D}\left[\frac{1}{2} - \left(\beta - \frac{1}{2}\gamma\right) 2\xi\Omega_0\right](\Delta t)^2 a_i \\ &\quad + \frac{\beta}{D}\frac{1}{m}(\Delta t)^2 (f_{i+1} - f_i) \\ &\quad - \frac{\beta}{D}\left[\Omega_i^2 d_i + 2\xi\Omega_i (\Delta t)\, v_i \right. \\ &\quad \left. + (\Delta t)^2 a_i - \frac{1}{m}(\Delta t)^2 f_i\right] \\ &= d_i + \frac{1}{D}\left(1 + 2\gamma\xi\Omega_0\right)(\Delta t)\, v_i \\ &\quad + \frac{1}{D}\left[\frac{1}{2} - \left(\beta - \frac{1}{2}\gamma\right) 2\xi\Omega_0\right](\Delta t)^2 a_i \\ &\quad + \frac{\beta}{D}\frac{1}{m}(\Delta t)^2 (f_{i+1} - f_i) \end{aligned} \tag{60}$$

where the second line of this equation is equal to zero since the dynamic equilibrium must be met at the ith time step. As a result, the third line of this equation becomes the displacement difference equation of this non-dissipative family of methods and then Eq. (59) will be simplified to be:

$$\begin{aligned} \bar{\beta}_1 &= 0 \\ \bar{\beta}_2 &= \frac{1}{D}\left(1 + 2\gamma\xi\Omega_0\right) \\ \bar{\beta}_3 &= \frac{1}{D}\left[\frac{1}{2} - \left(\beta - \frac{1}{2}\gamma\right) 2\xi\Omega_0\right] \\ \bar{p}_{i+1} &= \frac{1}{D}\beta\frac{1}{m}(\Delta t)^2 (f_{i+1} - f_i) \end{aligned} \tag{61}$$

This family of methods is the same as that presented in [30]. In addition, the choice of $\beta = 1/4$ and $\gamma = 1/2$ reduces to the Chang explicit method [27] and the choice of $\beta = \gamma = 1/2$ becomes the improved Chang explicit method [29].

Although the study of CAM in this work focuses on the family of one-step integration methods the results are applicable to the corresponding family of two-step integration methods. This is because that the second line of Eq. (2) is numerically equivalent to Eq. (4) in addition to the same asymptotic equation of motion and velocity difference equation. This implies that each member of CAM of the family of one-step integration methods also corresponds to a member of the family of two-step integration methods. Hence, CAM is a dual family of integration methods.

10 Conclusions

A new family of structure-dependent integration methods is presented. This family of methods is generally a two-step method at the development stage, which covers most currently available semi-explicit structure-dependent integration methods. It can be further transformed into a one-step method by way of an ingenious arrangement of the asymptotic equation of motion. As a one-step integration method, it is a brand-new family of structure-dependent integration methods and thus it is thoroughly explored herein. Two important techniques have been used to develop this family of methods. A loading term is added into the displacement difference equation to eliminate an adverse high-frequency overshoot in steady-state responses, which is often found for a structure-dependent integration method. In addition, a stability amplification factor is also applied to improve stability properties so that there will be no constraint on the step size for solving inertial problems. This is because that structure-dependent integration methods generally have unconditional stability for linear elastic and stiffness softening systems, while they become conditionally stable for stiffness hardening systems. Hence, the proposed family of methods can have desirable numerical properties, such as unconditional stability, second-order accuracy, explicitness of each time step, and numerical dissipation. The numerical properties are the same as those of the generalized-α method for linear elastic systems for $\sigma = 1$. Notice that the proposed family of methods has no adverse properties that have been found in some structure-dependent integration methods, such as a weak instability, a high-frequency overshoot in steady-state responses, a conditional stability for stiffness hardening systems and a poor capability of seizing the rapid variation of structural nonlinearity.

The proposed family of methods and its two dissipative subfamilies of methods can have a favorable numerical damping. In general, the amount of numerical damping can be continuously controlled by a free parameter and it is possible to achieve zero numerical damping. This numerical damping can be used to repress or even remove the spurious oscillations

of high-frequency modes, while the low-frequency responses are almost unaffected. In contrast to the generalized-α method, the most important improvement of this family of methods is that it is a semi-explicit method. In general, it involves no nonlinear iterations per time step, and thus it can save many computationally efforts. An example shows that the CPU time consumed by the proposed family of methods is only about 1% of that consumed by the generalized-α method for a 200-degree-of-freedom system, and it reduces to about 0.26% for a 1600 degrees of freedom system. Clearly, the computational efficiency generally increases with the total number of the degree of freedom. The cause of this computational efficiency is also fully explored by considering the computations that consume major computational efforts at each time step.

Acknowledgements The author is grateful to acknowledge that this study is financially supported by the Ministry of Science and Technology, Taiwan, R.O.C., under Grant No. MOST-107-2221-E-027-011.

References

1. Houbolt, J.C.: A recurrence matrix solution for the dynamic response of elastic aircraft. J. Aeronaut. Sci. **17**, 540–550 (1950)
2. Newmark, N.M.: A method of computation for structural dynamics. J. Eng. Mech. Div. **85**(3), 67–94 (1959)
3. Wilson, E.L., Farhoomand, I., Bathe, K.J.: Nonlinear dynamic analysis of complex structures. Earthq. Eng. Struct. Dyn. **1**, 241–252 (1973)
4. Park, K.C.: An improved stiffly stable method for direct integration of nonlinear structural dynamic equations. J. Appl. Mech. **42**, 464–470 (1975)
5. Hilber, H.M., Hughes, T.J.R., Taylor, R.L.: Improved numerical dissipation for time integration algorithms in structural dynamics. Earthq. Eng. Struct. Dyn. **5**, 283–292 (1977)
6. Wood, W.L., Bossak, M., Zienkiewicz, O.C.: An alpha modification of Newmark's method. Int. J. Numer. Methods Eng. **15**, 1562–1566 (1981)
7. Chung, J., Hulbert, G.M.: A time integration algorithm for structural dynamics with improved numerical dissipation: the generalized-α method. J. Appl. Mech. **60**(6), 371–375 (1993)
8. Chang, S.Y.: Improved numerical dissipation for explicit methods in pseudodynamic tests. Earthq. Eng. Struct. Dyn. **26**, 917–929 (1997)
9. Tamma, K.K., Sha, D., Zhou, X.: Time discretized operators. Part 1: towards the theoretical design of a new generation of a generalized family of unconditionally stable implicit and explicit representations of arbitrary order for computational dynamics. Comput. Methods Appl. Mech. Eng. **192**, 257–290 (2003)
10. Sha, D., Zhou, X., Tamma, K.K.: Time discretized operators. Part 2: Towards the theoretical design of a new generation of a generalized family of unconditionally stable implicit and explicit representations of arbitrary order for computational dynamics. Comput. Methods Appl. Mech. Eng. **192**, 291–329 (2003)
11. Zhou, X., Tamma, K.K.: Design, analysis, and synthesis of generalized single step single solve and optimal algorithms for structural dynamics. Int. J. Numer. Methods Eng. **59**, 597–668 (2004)
12. Zhou, X., Tamma, K.K., Sha, D.: Design spaces, measures and metrics for evaluating quality of time operators and consequences leading to improved algorithms by design-illustration to structural dynamics. Int. J. Numer. Methods Eng. **64**, 1841–1870 (2005)
13. Fung, T.C.: Complex time-step Newmark methods with controllable numerical dissipation. Int. J. Numer. Methods Eng. **41**, 65–93 (1998)
14. Chang, S.Y.: The γ-function pseudodynamic algorithm. J. Earthq. Eng. **4**(3), 303–320 (2000)
15. Armero, F., Romero, I.: On the formulation of high-frequency dissipative time-stepping algorithms for nonlinear dynamics. Part II: second-order methods. Comput. Methods Appl. Mech. Eng. **190**, 6783–6824 (2001)
16. Krenk, S.: Energy conservation in Newmark based time integration algorithms. Comput. Methods Appl. Mech. Eng. **195**, 6110–6124 (2006)
17. Lopez, S.: Changing the representation and improving stability in time-stepping analysis of structural non-linear dynamics. Nonlinear Dyn. **46**, 337–348 (2006)
18. Lopez, S.: Relaxed representations and improving stability in time-stepping analysis of three- dimensional structural nonlinear dynamics. Nonlinear Dyn. **69**, 705–720 (2012)
19. Soares, D.: An explicit family of time marching procedures with adaptive dissipation control. Int. J. Numer. Methods Eng. **100**, 165–182 (2014)
20. Wang, J., Li, Z.: Implementation of HHT algorithm for numerical integration of multibody dynamics with holonomic constraints. Nonlinear Dyn. **80**, 817–825 (2015)
21. Soares, D.: A simple and effective new family of time marching procedures for dynamics. Comput. Methods Appl. Mech. Eng. **283**, 1138–1166 (2015)
22. Belytschko, T., Hughes, T.J.R.: Computational Methods for Transient Analysis. Elsevier Science Publishers B.V, North-Holland (1983)
23. Hughes, T.J.R.: The Finite Element Method. Prentice-Hall Inc, Englewood Cliffs (1987)
24. Har, J., Tamma, K.K.: Advances in Computational Dynamics of Particles, Materials and Structures. Wiley, New York (2012)
25. Lax, P.D., Richmyer, R.D.: Survey of the stability of linear difference equations. Commun. Pure Appl. Math. **9**, 267–293 (1956)
26. Dahlquist, G.: A special stability problem for linear multistep methods. BIT **3**, 27–43 (1963)
27. Chang, S.Y.: Explicit pseudodynamic algorithm with unconditional stability. J. Eng. Mech. ASCE **128**(9), 935–947 (2002)
28. Chang, S.Y.: Improved explicit method for structural dynamics. J. Eng. Mech. ASCE **133**(7), 748–760 (2007)

29. Chang, S.Y.: An explicit method with improved stability property. Int. J. Numer. Method Eng. **77**(8), 1100–1120 (2009)
30. Chang, S.Y.: A new family of explicit method for linear structural dynamics. Comput. Struct. **88**(11–12), 755–772 (2010)
31. Chang, S.Y.: Discussion of paper 'Real-time hybrid testing using the unconditionally stable explicit CR integration algorithm' by Cheng Chen, James M. Ricles, Thomas M. Marullo and Oya Mercan. Earthq. Eng. Struct. Dyn. **41**, 1061–1063 (2012)
32. Gui, Y., Wang, J.T., Jin, F., Chen, C., Zhou, M.X.: Development of a family of explicit algorithms for structural dynamics with unconditional stability. Nonlinear Dyn. **77**(4), 1157–1170 (2014)
33. Chang, S.Y.: Family of structure-dependent explicit methods for structural dynamics. J. Eng. Mech. ASCE **140**(6), 06014005 (2014)
34. Tang, Y., Lou, M.L.: New unconditionally stable explicit integration algorithm for real-time hybrid testing. J. Eng. Mech. ASCE **143**(7), 04017029 (2017)
35. Chang, S.Y.: A family of non-iterative integration methods with desired numerical dissipation. Int. J. Numer. Methods Eng. **100**(1), 62–86 (2014)
36. Chang, S.Y.: Dissipative, non-iterative integration algorithms with unconditional stability for mildly nonlinear structural dynamics. Nonlinear Dyn. **79**(2), 1625–1649 (2015)
37. Chang, S.Y.: Discussion of paper 'Development of a family of unconditionally stable explicit direct integration algorithms with controllable numerical energy dissipation' by Chinmoy Kolay and James M. Ricles. Earthq. Eng. Struct. Dyn. **44**(2), 325–328 (2015)
38. Chang, S.Y.: Assessments of dissipative structure-dependent integration methods. Struct. Eng. Mech. **62**(2), 151–162 (2017)
39. Chang, S.Y.: A general technique to improve stability property for a structure-dependent integration method. Int. J. Numer. Methods Eng. **101**(9), 653–669 (2015)
40. Chang, S.Y.: An unusual amplitude growth property and its remedy for structure-dependent integration methods. Comput. Methods Appl. Mech. Eng. **330**, 498–521 (2018)
41. Goudreau, G.L., Taylor, R.L.: Evaluation of numerical integration methods in elasto-dynamics. Comput. Methods Appl. Mech. Eng. **2**, 69–97 (1972)
42. Hilber, H.M., Hughes, T.J.R.: Collocation, dissipation, and 'overshoot' for time integration schemes in structural dynamics. Earthq. Eng. Struct. Dyn. **6**, 99–118 (1978)
43. Chang, S.Y.: Accurate representation of external force in time history analysis. J. Eng. Mech. ASCE **132**(1), 34–45 (2006)
44. Chang, S.Y.: Performances of non-dissipative structure-dependent integration methods. Struct. Eng. Mech. **65**(1), 91–98 (2018)
45. Chang, S.Y.: Weak instability of CR explicit method for structural dynamics. J. Comput. Nonlinear Dyn. **13**(5), 054501 (2018)
46. Chang, S.Y.: Choices of structure-dependent pseudodynamic algorithms. J. Eng. Mech. ASCE **145**(5), 04019029 (2019)
47. Chang, S.Y., Veerarajan, S., Wu, T.H.: Discussion of paper 'Improved explicit integration algorithms for structural dynamic analysis with unconditional stability and controllable numerical dissipation' by Chinmoy Kolay and James M. Ricles. J. Earthq. Eng. (2019). https://doi.org/10.1080/13632469.2019.1662345
48. Geradin, M., Rixen, D.: Mechanical Vibrations Theory and Application to Structural Dynamics. Wiley, New York (1994)